AFRL-SR-BL-TR-02-

0116

REPORT DOCUMENTATION PAGE

1. REPORT DATE *(DD-MM-YYYY)*	2. REPORT TYPE	3. DATES COVERED *(From-To)*
15-02-2002	Final progress report	12-01-00 – 11-31-2001

4. TITLE AND SUBTITLE
High temperature optical fiber instrumentation for gas flow monitoring in gas turbine engines

5a. CONTRACT NUMBER

5b. GRANT NUMBER
F49620-01-1-0016

5c. PROGRAM ELEMENT NUMBER

6. AUTHOR(S)
Anbo Wang
Gary Pickrell
Russell May
Adrian Roberts

5d. PROJECT NUMBER

5e. TASK NUMBER

5f. WORK UNIT NUMBER

7. PERFORMING ORGANIZATION NAME(S) AND ADDRESS(ES)
Center for Photonics Technology
Virginia Polytechnic Institute and State University
460 Turner Street, Suite 303
Blacksburg, VA 24060

8. PERFORMING ORGANIZATION REPORT NUMBER

9. SPONSORING/MONITORING AGENCY NAME(S) AND ADDRESS(ES)
Air Force Office of Scientific Research

10. SPONSOR/MONITOR'S ACRONYM(S)
AFOSR

11. SPONSOR/MONITOR'S REPORT NUMBER(S)

12. DISTRIBUTION/AVAILABILITY STATEMENT

DISTRIBUTION STATEMENT A
Approved for Public Release
Distribution Unlimited

13. SUPPLEMENTARY NOTES

14. ABSTRACT
Fiber optic sensors have now been used for medical, chemical and biomedical applications and to measure pressure, temperature and strain in a number of different industries. In order to use one of the techniques utilized in fiber optic sensing, a design must be chosen which is capable of making absolute measurements with a high accuracy, and high data rates. The sensor technology chosen here is the self-calibrated interferometric/intensity-based (SCIIB) optical fiber sensor. This document discusses the initial stages of the development of an SCIIB system to meet the requirements for pressure measurement in gas turbine engines. It was possible to show that a tube-based sensor could be modified to generate an increased frequency response, however it came at the cost of increased temperature sensitivity and a lack of repeatable results.

15. SUBJECT TERMS

16. SECURITY CLASSIFICATION OF:			17. LIMITATION OF ABSTRACT	18. NUMBER OF PAGES	19a. NAME OF RESPONSIBLE PERSON
a. REPORT	b. ABSTRACT	c. THIS PAGE			Anbo Wang
				60	19b. TELEPHONE NUMBER *(Include area code)* (540)-231-4355

High-temperature Optical Fiber Sensor Instrumentation for Gas Flow Monitoring in Gas Turbine Engines

Final Performance Report

AFOSR Award Number – F49620-01-1-0016

Reporting Period Start Date – 1 December 2000
Reporting Period Stop Date – 30 November 2001

Prepared by: A.Wang, G. Pickrell, A. Roberts and R. May
Report Issued: 28, February 2002

Submitted by: Center for Photonics Technology
Bradley Department of Electrical and Computer Engineering
Virginia Tech - M/C 0111
Blacksburg, VA 24061

CPT
CENTER FOR PHOTONICS TECHNOLOGY

Table of Contents

Table of Contents....ii

List of Figures....iv

List of Tables....v

1. Introduction....1
1.1 Pressure....1
1.2 Gas Turbine Engines....1
1.3 Pressure Sensor Choices....3
1.4 Design Parameters....3

2. Theory....5
2.1 Extrinsic Fabry-Pérot Interferometric Cavity....5
2.2 Intensity-based Optical Fiber Sensor System....6
2.3 SCIIB Optical Fiber Sensor System....7
2.3.1. Introduction to the SCIIB System....7
2.3.2. SCIIB Pressure Sensors....8

3. Sensor Design....10
3.1 Gage Length....10
3.2 Initial Airgap....10
3.3 Frequency Response....11
3.3.1. Mass on a Spring Model....12
3.3.2. Sensitivity Model....12
3.3.3. Selection of a Model....13

4. Sensor Fabrication....15
4.1 Sensor Head Fabrication System....16
4.2 Fabrication Procedure....17
4.3 Sensor Head Modifications to Enable Higher Frequency Response....18

5. Pressure System Design....20
5.1 Pressure System Hardware....20
5.2 Pressure System Software....22

6. Preliminary results....24
6.1 Design Results....24
6.2 Comparison of Intensity-Based and SCIIB Fiber Sensors....25
6.3 Trial of the Experiment....26

7. Experiment....28
7.1 Pressure System Setup....28
7.1.1. System Setup....28
7.1.2. Procedure....28
7.2 Sensor System....28

7.2.1. System Setup..... 28
7.2.2. Procedure..... 29
7.3 Calibration..... 29
7.4 Data Acquisition..... 29
7.5 Post-Processing..... 30
7.5.1 Low-Pass Filter Design Considerations..... 31
7.5.2 Frequency Response Considerations..... 32

8. Results..... 34
8.1 Room-Temperature Experimental Results..... 34
8.2 High-Temperature Experimental Results..... 36
8.2.1 Results at 300 °F..... 37
8.2.2 Results at 500 °F..... 39
8.3 Sensor Resolution..... 41
8.4 Temperature Effects..... 42

9. Conclusions and Suggestions for Future Work..... 44
9.1 Conclusions..... 44
9.2 Suggestions for future Work..... 45

10. References..... 46

Appendices

List of Figures

Figure 1.1: Simplified diagram of a gas turbine engine..... 2
Figure 1.2: Diagram of a turbofan engine..... 2
Figure 2.1: Extrinsic Fabry-Pérot Interferometric Sensor..... 5
Figure 2.2: Schematic diagram of an intensity based system..... 6
Figure 2.3: Illustration of the principle of the self-calibrated interferometric/intensity-based (SCIIB) optical fiber sensor system..... 7
Figure 3.1: Diagram showing how the intensity in the narrowband channel varies with change in airgap..... 11
Figure 4.1: Functional block diagram of the SCIIB sensor fabrication system..... 16
Figure 4.2: Sensor fabrication equipment..... 17
Figure 4.3: Microscopic photograph of the SCIIB sensor head..... 18
Figure 5.1: Schematic block diagram of the pressure chamber design..... 20
Figure 5.2: Photograph of the experimental setup..... 21
Figure 5.3: Screen capture of the pressure control unit LABView graphical user interface..... 22
Figure 6.1: Comparison of the stability obtained by switching to SCIIB system..... 25
Figure 6.2: Data collected to verify that the pressure system worked as designed..... 26
Figure 6.3: Photograph of a ruptured diaphragm..... 27
Figure 7.1: Screen capture of the data acquisition LABView graphical user interface..... 30
Figure 7.2: Block diagram of the DSP algorithm used to process the voltage output of the SCIIB system..... 31
Figure 7.3: Sampled sensor output for ideal cases..... 32
Figure 7.4: Frequency domain analysis of the sensor output voltage..... 33
Figure 8.1: Room temperature pressure calibration curve..... 34
Figure 8.2: Room temperature SCIIB optical fiber sensor output and the pressure calibration unit data plotted on the same axes..... 35
Figure 8.3: Close up view of the output voltage at the time of the rupture..... 36
Figure 8.4: Calibration curves for the sensor with the 220 μm outer diameter at 300 °F outer temperature..... 37
Figure 8.5: SCIIB optical fiber sensor output at 300 °F plotted together with the pressure calibration unit data..... 38
Figure 8.6: Room temperature sensor data generated using the calibration curve in Section 8.1..... 38
Figure 8.7: Close up view of the output voltage at the time of the rupture. This was used to determine the sensor frequency response..... 39
Figure 8.8: Calibration curve for the sensor with the 220 μm outer diameter at 500 °F outer temperature..... 40
Figure 8.9: Two trials o f the SCIIB optical fiber sensor output at 500 °F plotted together with the corresponding pressure calibration unit data..... 40
Figure 8.10: Close up view of the output voltage at the time of the rupture..... 41
Figure 8.11: Plots demonstrating the improvement once the noise was isolated..... 42
Figure 8.12: Voltage output of the SCIIB sensor when the temperature is decreased from 300 °F, to room temperature..... 43

List of Tables

Table 1.1: Table summarizing the given design specifications..... 4
Table 5.1: Modes of Operation of the pressure control unit software..... 23
Table 6.1: Comparison of experimental results and the sensor design program..... 24
Table 6.2: Comparison of experimental results the modified sensor design program..... 24
Table 8.1: Sensor Parameters..... 34
Table 8.2: Comparison of temperature inside the chamber to reading from the outside..... 36
Table 8.3: Standard deviation of the sensor output for room temperature measurements..... 41
Table 8.4: Standard deviation of the sensor output for high temperature measurements..... 42
Table 9.1: Summary of the targets and the results obtained..... 44

1. Introduction

1.1 Pressure

Pressure can be thought of as the perpendicular force exerted on a unit area. For example, atmospheric pressure (the force exerted by the weight of the atmosphere) at sea level is usually stated as 15 pounds per square inch (*psi*). This means that the column of air with a footprint of one square inch exerts a 15-pound force on the earth's surface at sea level.

As is the case with many readings, like voltage and temperature, it is necessary to have a common reference so that all readings are standard. Obviously this will enable anyone to refer to measurements made and be understood worldwide. In the case of temperature, it is know that 0 °C corresponds to the freezing/melting point of water and 0 K corresponds to the temperature at which all molecular motion ceases. Similarly with absolute pressure, 0 psi corresponds to the pressure in a vacuum. This means that an absolute pressure reading will include a component which is due to atmospheric pressure. Many technologies are currently in use for performing this measurement, including deflection of stainless steel diaphragms, semiconductor hybrid sensors, micro electromechanical machined sensors, and optical fiber sensors. However, it will be seen from the description below that some of these technologies are not suited to performing pressure measurement in a gas turbine engine.

1.2 Gas Turbine Engines

Figure 1.1 is a simplified diagram of a gas turbine engine. Depicted in this image are the three main stages: the compressor, the combustion area, and the turbines. Each area is described in more detail below.

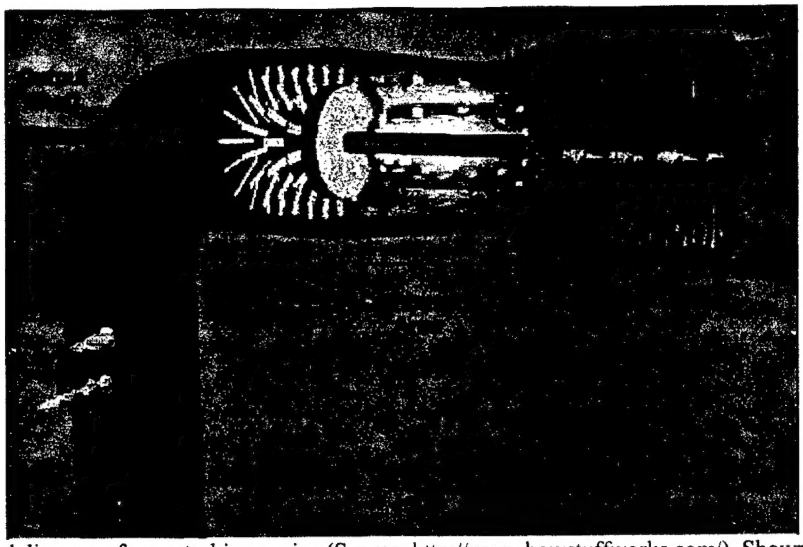

Figure 1.1: Simplified diagram of a gas turbine engine (Source: http://www.howstuffworks.com/). Shown here are the three main parts of a gas turbine engine: the compressor, the combustion area and the turbines.

The air enters the engine through the compressor. The compressor is essentially a cone-shaped cylinder with fan blades inside. When the outside air is forced through the compressor stage, the pressure increases dramatically (up to 30 times in some engines). This compressed air then enters the combustion area, where it is heated by a flame which is burning behind a "flame holder". The heated air then passes through the blades of the turbine, causing them to turn, and then exits the engine in the form of exhaust. The final stage of the turbine is used to drive a shaft, which is then used to generate power. In aircraft, a piece needs to be added to this diagram in order to create a turbofan. Figure 1.2 is a diagram of the turbofan, which uses a gas turbine engine.

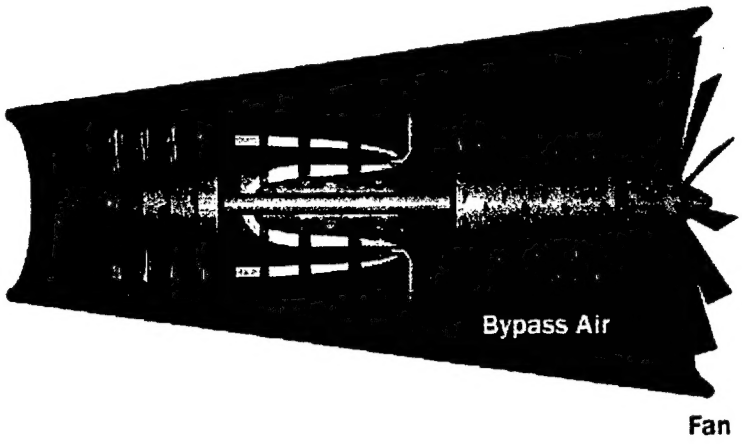

Figure 1.2: Diagram of a turbofan engine (Source: http://howstuffworks.com/).

In a turbofan engine, the shaft is used to power a fan, which is forced out of the rear of the engine along with the exhaust from the engine. The large volume of air moved by the fan located at the front of the engine, combined with the exhaust, provides a large amount of thrust for the aircraft.

Sensors will need to be placed along the walls of the gas turbine engine to make pressure measurements while the turbine is running. This introduces many concerns.

1. Can the sensor survive the high temperatures, if it is measuring pressure in or near the combustion area?
2. Can the lead to the sensor survive the environment which it will be exposed to (both the high temperature and the fast-flowing air if located in a turbofan engine)?
3. Can the sensor respond to the rapid changes in pressure caused by the passing fan blades?
4. Can the sensor produce reliable pressure readings if the temperature fluctuates?

1.3 Pressure Sensor Choices

The above-mentioned environment will be a challenge to many of the sensor technologies currently in use today. As can be seen from the above description, the sensors will need to be able to survive pressures which are tens of times greater than atmospheric pressure, and it will need to be able to resolve rapid variations in pressure caused by the passing of fan blades. The other concern will be the sensor's ability to survive high temperature environments. Semiconductor material will not perform well under the high temperature environment, and the stainless steel sensors will need complicated compensation for variations in temperature when measuring pressure. The optical fiber sensors have been proven to be able to give reliable readings in harsh environments, and can be designed to exhibit only a small temperature dependence. When coupled with the accuracy of the SCIIB system, these sensors ideally fit the requirements.

1.4 Design Parameters

The design specifications given for this project are as follows:

Table 1.1: Table summarizing the given design specifications

PARAMETER	SPECIFICATION
Maximum pressure to be measured	150 psi
High-frequency pressure component	5 psi
Maximum temperature to withstand	500 °F
Blade passing frequency	6 – 17 kHz
Desired resolution	0.1% ≈ 0.1psi
Desired sensor frequency response	150kHz
Distance out of "hot zone"	2 m

Source: Dick Rivir of the Air Force Research Laboratory

In previous work performed at the Center for Photonics Technology, an SCIIB system was able to demonstrate a frequency response of 15 kHz and a resolution of 1 psi. This means that the system design needs to improve upon both the frequency response and the resolution by a factor of 10.

2. Theory

The sensor present in the SCIIB system is an extrinsic Fabry-Pérot interferometer (EFPI). This light interferometric method allows the sensor to measure the displacement between two cleaved fiber end-faces with a precision comparable to a fraction of the wavelength. By causing variations in the cavity length and measuring this displacement, it is possible to use this structure to determine strain [3], temperature, pressure, acoustics and many other variables [2]. The basic structure of this sensor is presented in Section 2.1.

2.1 Extrinsic Fabry-Pérot Interferometric Cavity

Figure 2.1 is an illustration of an EFPI cavity. Depicted here are the lead-in fiber, the reflecting fiber and the alignment tube. By aligning the two fiber end-faces and separating them by a specified distance, the structure takes on the properties discussed by physicist L. Fabry Pérot in the *Journal of Physics*, 1898 [4].

In this application, light is transmitted down the lead-in fiber and it impinges upon the glass-air interface (i.e. where the airgap meets the cleaved surface of the lead-in fiber). Assuming that the fiber is made of fused-silica fiber, about 4% of the energy is reflected (labeled as *R1* in Figure 2.1), while the remainder propagates across the airgap to the air-glass interface at the cleaved end-face of the reflecting fiber. 4% of the incident energy then propagates back to the air-glass interface at the cleaved end-face of the lead-in fiber [5]. Transmission and reflection also occur at this interface in the proportions previously mentioned, and the two signals (*R1* and *R2*) interfere.

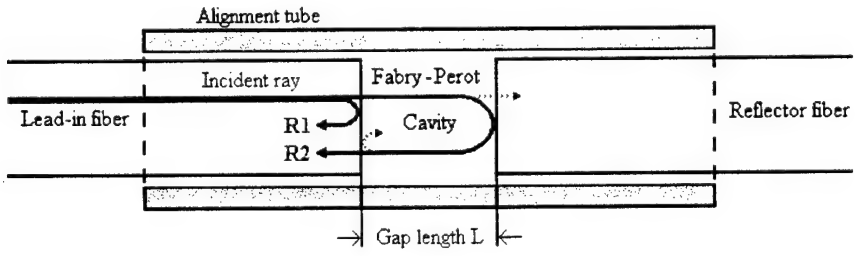

Figure 2.1: Extrinsic Fabry-Pérot Interferometric Sensor.

Changes in the airgap get encoded in this signal because of the differences in the optical path-length of R1 and R2. The intensity equation presented in Equation 2.1, shows the relationship between the airgap and the received light intensity:

$$I(x) = I_0(x)\left[1 + \gamma(d)\cos\left(\frac{4\pi d}{\lambda_C}\right)\right] \qquad (2.1)$$

where,

$\gamma(d) = 2\,\Omega(\mathrm{d}) / (1 + \Omega(\mathrm{d})^2)$

$\Omega(d)$ losses dependent on the reflection, and transmission coefficients at the air-glass interfaces, and on the attenuation of R2

$I_0(x)$ initial light intensity

This relationship can be used to show that the light intensity varies as the airgap changes. However due to the ambiguity which is inherent in a sinusoidal waveform (i.e. a specific value of voltage corresponds to multiple airgap values – see Figure 3.1), difficulties in decoding the measured airgap occur. Solving this problem of ambiguity will be addressed in the following sections.

2.2 Intensity-based Optical Fiber Sensor System

Figure 2.2 shows a schematic block diagram of an intensity-based system.

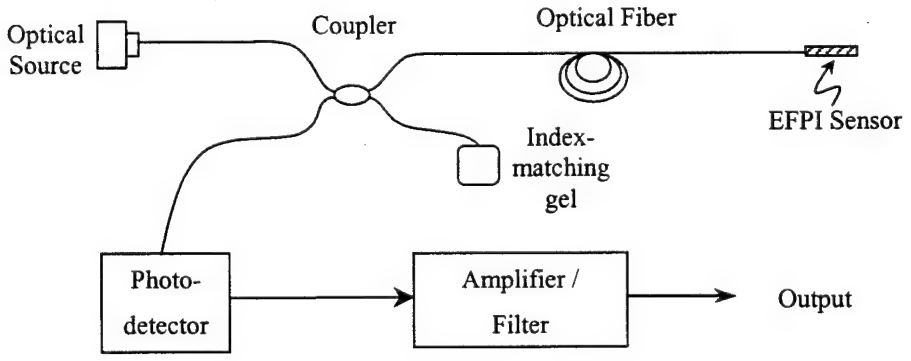

Figure 2.2: Schematic diagram of an intensity based system

In the system above, the light is coupled into the fiber from a narrowband optical source. This light travels through the coupler to the EFPI sensor where the interference explained in Section 2.1 occurs. This interference signal propagates back along the fiber to a photodetector, and then to a transimpedance amplifier / filter network. The output voltage varies with the light intensity and can be used to determine the change in airgap. This signal can be stored for later analysis or it can be monitored in real-time.

The problem of ambiguity mentioned in Section 2.1 will be overcome here by limiting the system to the linear range of the sensor (Figure 3.1). However other problems, most notably time-varying fiber losses, still exist with this configuration. These can come from fluctuations in the optical source power, or with time-varying fiber losses. These significant errors are the motivation behind the development of the SCIIB system.

2.3 SCIIB Optical Fiber Sensor System

2.3.1 Introduction to the SCIIB System

The following discussion can be found in greater detail, in the paper on SCIIB optical fiber sensors [6].

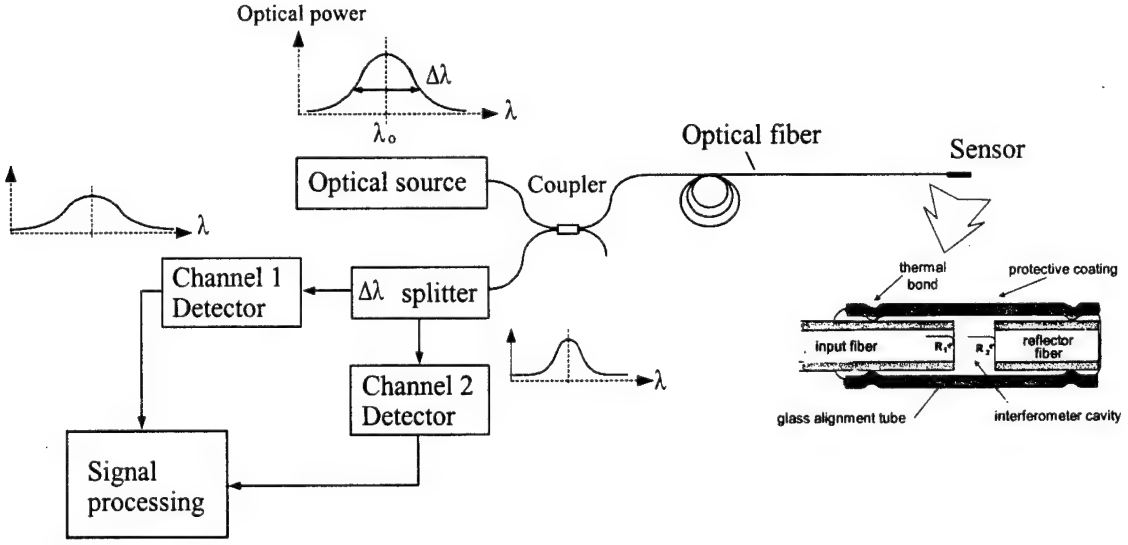

Figure 2.3: Illustration of the principle of the self-calibrated interferometric/intensity-based (SCIIB) optical fiber sensor system. The graphs illustrate the spectral power distribution of the optical source output and the transmittances of the two channels.

Figure 2.3 illustrates the SCIIB pressure sensor system. The system involves a sensor probe, an optoelectronic signal processing subsystem and an optical fiber linking the sensor head and signal processing unit. The light from a broadband optical source is launched into a two-by-two fiber coupler and propagates along the optical fiber to the sensor head. As shown in the enlarged view of the sensor head, the EFPI cavity is constructed by fusing the input fiber and a reflector fiber to a hollow glass tube. As explained in Section 2.1, the incident light is first partially reflected at the end-face of the input fiber. The remainder of the light propagates across the airgap to the reflector fiber end-face, where a second reflection is generated. The two reflections then travel back along the same input fiber through the same fiber coupler to the photodetection end.

One feature that makes the SCIIB system unique, is the splitting of this interference signal into two separate channels – a narrowband and a broadband channel. The airgap in the sensor head can be designed so that the difference in optical path length seen by each of the two interfering signals, is much smaller than the coherence length (Equation 2.2) of the narrowband signal but larger than that of the broadband signal.

$$L_{coherence} \approx \frac{\lambda_o^2}{\Delta\lambda} \qquad (2.2)$$

where,

$L_{coherence}$	coherence length
λ_o	center wavelength
$\Delta\lambda$	spectral width

This constraint causes changes in the airgap to be encoded in the narrowband channel but not the broadband signal. Therefore, the broadband channel can be used to remove variations in signal power which are not related to the changes in airgap. Among these are time-varying fiber losses, and fluctuations in the output power of optical source.

2.3.2 SCIIB Pressure Sensors

When a pressure is applied to the sensor head illustrated in Figure 2.2, the airgap separation in the sensor will change due to the longitudinal and lateral compression of the glass alignment tube. The airgap variation can be expressed as

$$\Delta d = \frac{L}{E} \frac{p r_0^2}{(r_0^2 - r_1^2)} (1 - 2\mu) \qquad (2.2)$$

where,

Δd	airgap variation
p	applied pressure
E	Young's modulus of the tube material
μ	Poisson ratio
L	distance between the two thermal fusion points
r_o and r_i	outer and inner radii of the glass tube, respectively

Equation (2.2) indicates that the airgap change is linear with respect to the applied pressure. In addition, the equation also shows the involvement of several sensor parameters, including the inner and outer diameters of the hollow glass tube, the distance between the two fusion points and the mechanical properties of the hollow glass material. The sensor thus offers excellent design flexibility for different dynamic measurement ranges.

3. Sensor Design

In the sensor design, normally there are two important design parameters. These are the gage length, and the initial airgap (or Fabry-Pérot cavity length). However, for this design the added parameter of the sensor frequency response has been added. The section below details the considerations made in calculating the above-mentioned parameters.

3.1 Gage Length

Sensor design starts at the airgap variation equation (2.2) and by solving this equation for gage length, we get:

$$L = \Delta d \frac{E}{p}\left(\frac{r_0^2 - r_i^2}{r_0^2}\right)\left(\frac{1}{(1-2\mu)}\right) \tag{3.1}$$

Assuming that the tube material and dimensions are fixed, it is possible to design the gage length by using the maximum values of airgap change and applied pressure (i.e. $\Delta d = \Delta d_{max}$ and $p = p_{max}$). For this application 200 psi will be used as the maximum pressure and the maximum change in airgap allowed depends on the center wavelength of the optical source.

3.2 Initial Airgap

Equation (3.3) shows the relationship between the source center wavelength (λ_C) and the maximum allowable change in airgap.

$$I = I_0\left[1 + \cos\left(\frac{4\pi d}{\lambda}\right)\right] \tag{3.2}$$

$$\Delta d_{max} = \frac{\lambda_C}{2\pi}\arcsin(0.6) \tag{3.3}$$

Equation (3.3) was derived from the simplified version of the intensity equation presented in equation (3.2). Since the initial tests will involve the use of an intensity-based system, it will be necessary to calculate the value of the initial airgap (d_0). d_0 can also be found by

manipulating the intensity equation. First the linear operation range of the sensor is determined (presented in Figure 3.1), then equation (3.2) is evaluated at both the minimum and the maximum values within this range. The result is presented as equation (3.4):

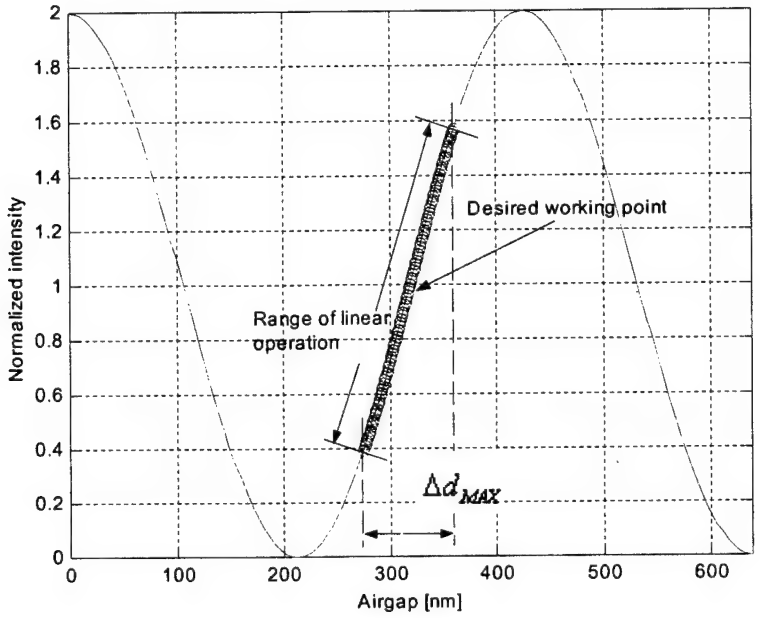

Figure 3.1: Diagram showing how the intensity in the narrowband channel varies with change in airgap. Also highlighted are the linear operation range for this sensor and the maximum allowable airgap change (λ_C = 850nm).

$$d_0 = \frac{\lambda}{4\pi}\arcsin\left(0.6\cdot\sin\left[\frac{4\pi\Delta d_{max}}{\lambda}\right]\right) \qquad (3.4)$$

Note: The previous design discussion assumes that the selected airgap value meets the criteria mentioned in Section 2.1. Namely that changes in the airgap are encoded in the narrowband channel, but not the broadband channel. The method of achieving this is also presented in [6].

3.3 Frequency Response

A model for frequency response had not been previously developed for these sensors. Hence it was necessary to develop an accurate model and two possibilities evolved. The first involved modeling the sensor as a mass on a spring and the frequency response was equated to the resonant frequency of this structure. The second model is based on determining the

sensitivity of the sensor from Equation 2.2. In both cases, it appeared that the alignment tube outer diameter needed to be modified in order to improve the sensor's frequency response or sensitivity.

3.3.1 Mass on a Spring Model

Modeling the sensor as a mass on a spring and calculating the natural frequency of the system yielded the equation below:

$$f = \frac{1}{2\pi}\sqrt{\frac{S_{tube} \cdot E}{L \cdot \rho \cdot (V_{tube} + V_{reflecting\ fiber})}} \tag{3.5}$$

where,

S_{tube} cross-sectional area of the glass tube

V_X volume of X

ρ density of the tube material

By noting the relationships between the frequency response and the various design parameters of the sensor (like the cross-sectional area of the tube, material properties and the length of the tube) some of the parameters for the fiber sensor were established. From the relationship above, it appears that if the sensor gage length is reduced, the resonant frequency will be increased. Also, it can be seen that by reducing the volume of the tube material and the volume of the reflecting fiber, the sensor frequency response will be increased. MATLAB code was generated to calculate this and a copy is presented in Appendix A.

3.3.2 Sensitivity Model

This model of the sensor mainly considers the sensitivity of the sensor. Analysis for this sensor begins at Equation 3.6, where the force seen by the sensor is a function of the applied pressure and the cross-sectional area of the glass tube.

$$F = p \cdot A \tag{3.6}$$

where,

F force applied by the pressure

p applied pressure

A cross-sectional area of the sensor

Further manipulation yields an equation for relating the measured pressure in terms of the applied pressure and the inner and outer radii of the alignment tube.

$$p_m = \frac{p}{r_o^2 - r_i^2} \tag{3.7}$$

where,

p_m measured pressure determined by using the SCIIB sensor

This indicates that as the outer and inner radii approach each other, an equal change in pressure causes a more significant change in the measure pressure. Physically this means that in order to increase the sensitivity of the sensor, either the alignment tube outer diameter needs to be reduced or its inner diameter needs to be increased.

One problem, with this model was that it was not possible to determine the sensitivity of the sensor just by giving the physical parameters of the sensor. The equation is more useful in explaining the sensitivity of the sensor qualitatively, than quantitatively.

3.3.3 Selection of a Model

In the first model, it was seen reducing the sensor gage length increases the frequency response. In order to change the sensor gage length and maintain the same linear operation region, the center wavelength of the source will have to be changed. However, the availability of parts will limit the choice of center frequency. Therefore, the volume of the tube material and the volume of the reflecting fiber will have to be reduced in order to facilitate a higher frequency response. This will be achieved by using sensors that are cut at the fusion point of the reflecting fiber and by reducing the outer diameter of the tubing (See Section 4).

For the second model, changing the inner diameter of the alignment tube will make the alignment less reliable and it may cause the sensor return misleading results for the change in

airgap. Hence the outer diameter of the alignment tube of the sensor needs be reduced. This will be accomplished as mentioned above.

Although the analyses methods were very different, both models yielded a similar result. Therefore the proof of one model being correct will come from experimentation and curve fitting.

As an aside, Equation 2.2 implies that changing the alignment tube outer diameter also changes other properties of the sensor. One such change is in the linear operating range of the sensor. Assuming a constant gage length (L), the linear range of the sensor will be change as the square of the outer radius divided by the difference between the inner and outer radii. This effect makes intuitive sense, because it is our position that reducing the outer diameter increases the sensitivity of the sensor (proven in later sections). The sensor therefore is more sensitive to small variations in the airgap, and thus the same change in pressure results in a voltage reading, which is further along the intensity curve (Figure 3.1). Therefore the linear range (shown in red) occurs over a smaller range of pressures, corresponding to a smaller operating range.

4. Sensor Fabrication

Once the sensor is designed, it will be necessary to fabricate it, such that the sensor output is optimized over the designed linear range. This is accomplished using accurate positioning stages, a microscope, and a carbon dioxide (CO_2) laser. Sensor fabrication is explained in detail in Hai Xiao's dissertation [4], and the method explained is similar to the method of construction used in this experiment. The only real difference was the use of the PZT – actuated stage in Xiao's work. In the work for this thesis, the positioning was performed using high-precision micrometers. To be complete a summary of the sensor fabrication described in the aforementioned reference is presented below.

Prior to the work done in the Center for Photonics Technology, the main method of creating an EFPI cavity involved bonding the fiber using epoxy. The problem with this method of construction is the limitation it places on the operating temperature of this sensor. Since the goal of this project will be to place the sensor in a turbine engine where the temperature can exceed 500 °C, it is mandatory to use this novel technique. Thermal fusion is used to bond the fiber and the alignment tube, and it enables the sensor to be used in temperatures in excess of 800 °C.

4.1 Sensor Head Fabrication System

The thermal fusion technique used in sensor head fabrication uses the sensor head fabrication system consisting of a carbon dioxide (CO_2) laser subsystem, a whitelight fiber optic interferometric subsystem and a X-Y translation stage. A diagram of the sensor fabrication system is presented in Figure 4.1.

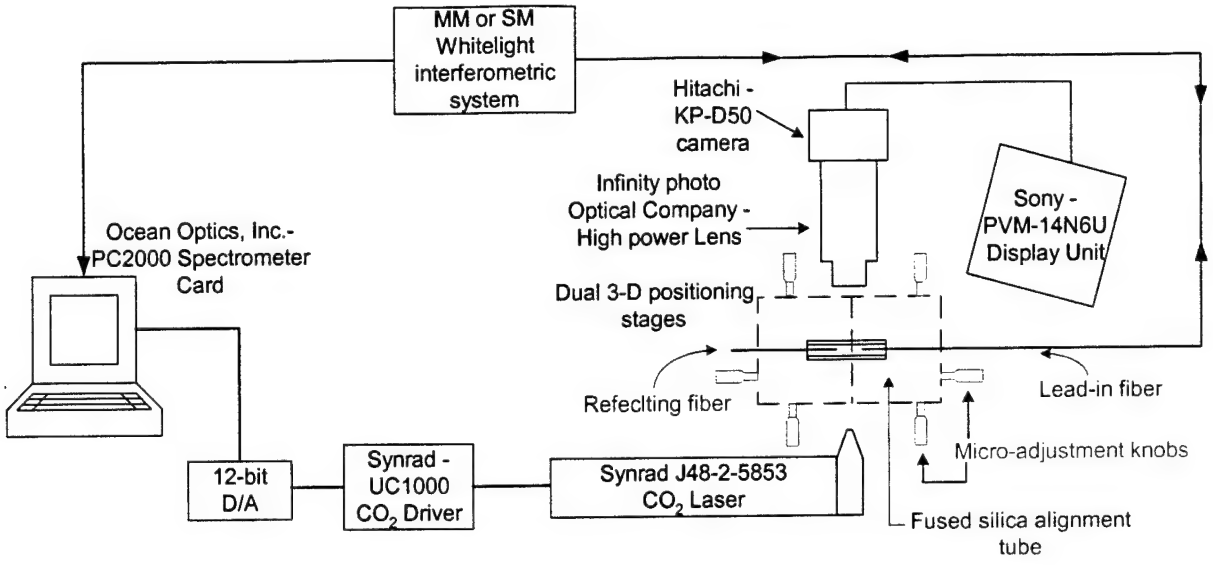

Figure 4.1: Functional block diagram of the SCIIB sensor fabrication system

Using the system shown in Figure 4.1, the sensors can be manufactured with very precise gage length (within 10 μm) by adjusting the micro-adjustment knobs and the desired airgap (within 0.01 nm) by repeatedly firing the laser at the fusion point of the reflecting fiber. A host computer is utilized in some aspects of the sensor head fabrication system. It controls the CO_2 laser operation, it reads the value of airgap, and displays the interference spectrum which is caused by the interference in the Fabry-Pérot cavity. The basic idea of the thermal fusion technique is as follows. A high-energy CO_2 laser works as the heating source which generates optical pulses at the central wavelength of 10.6 μm. When the silica fiber and tube are exposed to the CO_2 laser beam, they absorb the optical energy and convert it to thermal energy, which allows the silica fiber and tube to be bonded together by very high local temperature at the bonding point [4].

The Whitelight fiber optic interferometric system is used for accurately monitoring the value of airgap of the SCIIB sensor being fabricated. Two ultra-precise micro-positioning stages are also used in the system to allow precisely moving the input fiber and reflecting fiber in three dimensions. The functions and principles of these three sub-systems are discussed in detail in [4].

Figure 4.2 shows the actual setup of the equipment in the sensor fabrication room.

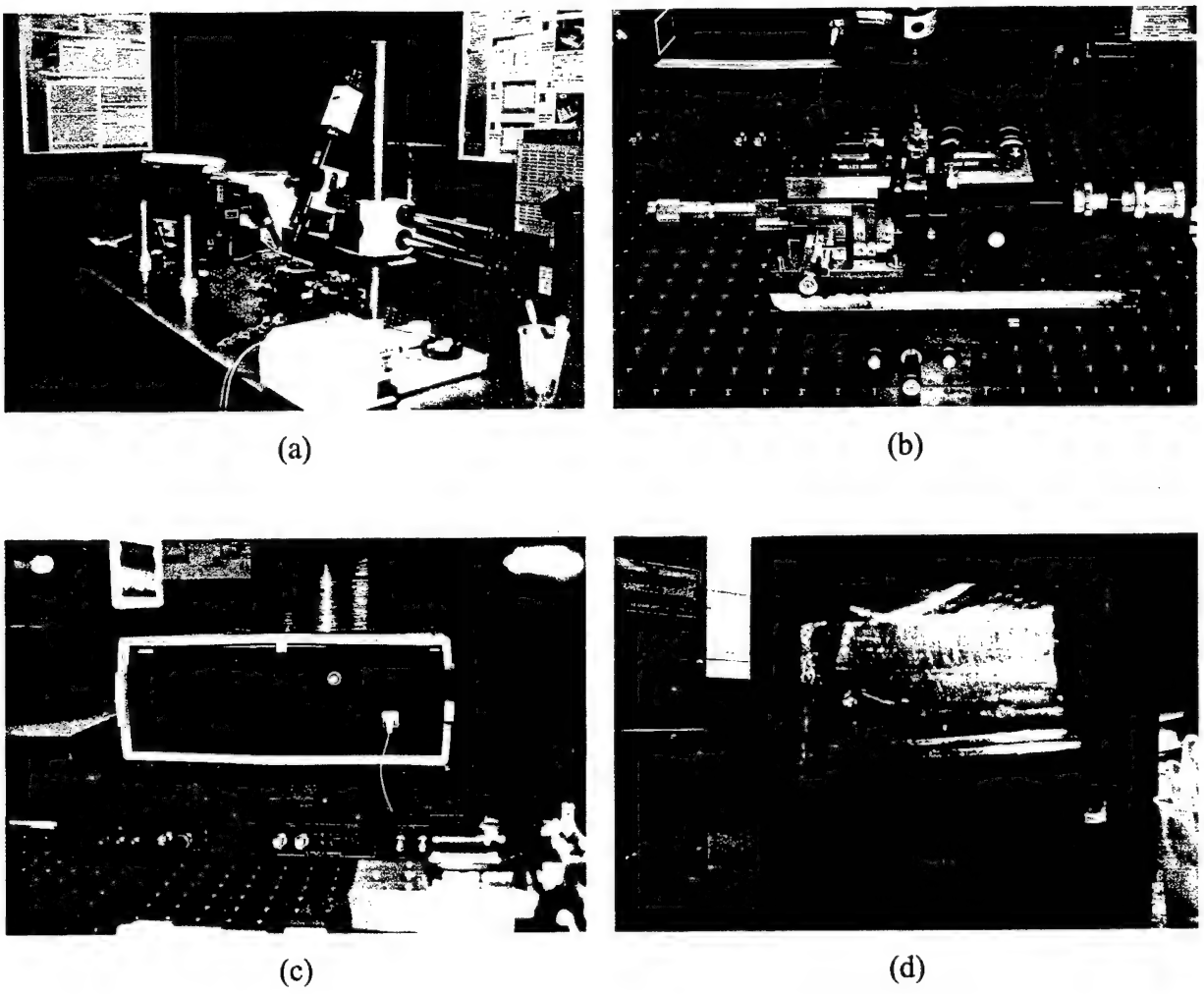

Figure 4.2: Sensor fabrication equipment. (a) Entire system shown in Figure 4.1. (b) 3-D dual positioning stages. (c) Whitelight interferometric unit. (d) CCD with image of the 360 μm capillary tube in the stages.

4.2 Fabrication Procedure

The steps to fabricating the highly precise SCIIB sensor heads are as follow:

1. Remove the buffer from the capillary tube (used as the glass alignment tube) and clean with a piece of dry tissue.
2. Cleave the tubing, place it in the 3-D positioning stage and secure it in place.
3. Remove the buffer from the end of the fiber. The length of the buffer to be removed is directly related to the desired sensor gage length and the desired length of the reflecting fiber (normally 4 – 10 cm).
4. Carefully clean this area using alcohol before cleaving using a fiber cleaver.

5. Using the microscope, align and insert the fiber into the capillary tube. Clamp the fiber to the 3-D positioning stage with magnetic holders.
6. Adjust the micro-adjustment knobs until the desired airgap is obtained. This requires moving the knobs slowly while monitoring the airgap using the Whitelight system display on the computer.
7. Adjust the 2-D translation stage underneath the micro-adjustment stage until the fiber and capillary tube assembly are at the center of the laser spot.
8. Use the CO_2 laser control software to perform thermal fusion (Section 4.2) at the lead-in fiber end of the capillary tube. It is necessary to select the power level and duration the CO_2 laser should be fired for good hermetically sealed sensor heads.
9. Move the fiber and capillary assembly to allow the reflecting and the capillary tube to be bonded using the 2-D translation stage. Repeat step 8.

Figure 4.4 is a photograph of a sensor which was made by following the procedures above.

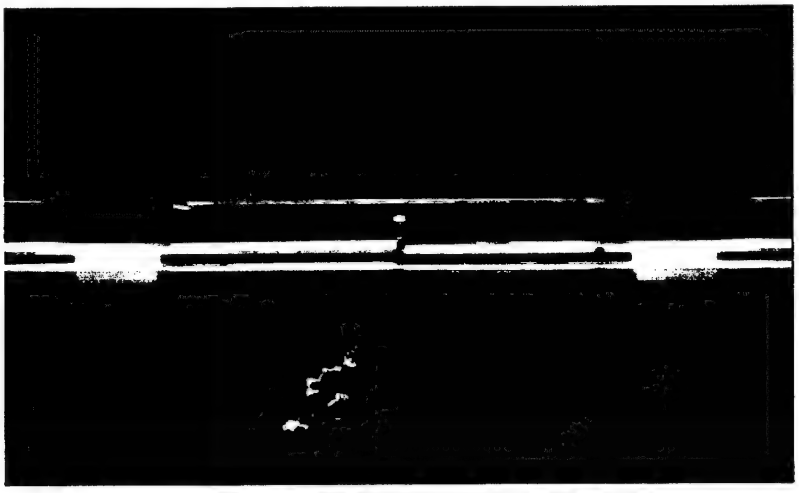

Figure 4.3: Microscopic photograph of the SCIIB sensor head

This picture clearly shows the fusion points of the lead-in and reflecting fiber and by carefully looking at the image, you can see the airgap in the center.

4.3 Sensor Head Modifications to Enable Higher Frequency Response

As mentioned in Section 3.4, in order to increase the frequency response of the sensor, it will be necessary to decrease the sensor outer diameter. This was accomplished by etching the sensor head after the sensor was fabricated. The sensor was placed in a 50% hydrofluoric acid solution for a period of 45 minutes, to reduce the outer diameter from 360 μm to 220 μm.

After the etching was performed, the sensor was cleaned and the outer diameter was measured using, the 3-D positioning stages, the camera and the CCD display unit. In order to measure the outer diameter with this equipment, the sensor was placed in the 3-D positioning stages, and a piece of tape was used to mark the one side of the glass alignment tube on the CCD screen. Then the reading of the micrometer on the stage was recorded. The position was then adjusted so that the other side of the glass alignment tube would line up with the tape, and the new reading was recorded. The difference between these two readings gives the outer diameter of the alignment tube, but since this is a measurement which is performed by human perspective, it is difficult to determine the tolerance. Based on the resolution of the camera and the fine adjustment possible when turning the adjustment knobs, it is apparent that the error is on the order of a few microns. Therefore, the values of the tube outer diameter presented in Section 8 are only rough measurements, and a tolerance of $\pm$ 5μm will be assumed.

5. Pressure System Design

5.1 Pressure System Hardware

Normally the frequency response of a system is defined according to the frequency of the sinusoidal waveform that can be resolved by said system. In some cases it is further implied that sensor frequency is determined by applying the Nyquist dictate, that the frequency response is ½ the rate at which you are able to sample. However, since a sinusoidal pressure with a high frequency cannot be developed in the lab, it was necessary to generate a signal with high-frequency content and then perform analysis in the frequency domain. This meant that the system needed to generate an impulse or a step in pressure, and the resolution of the edge will determine the frequency response of the sensor.

In order to achieve this, an instantaneous change in pressure was generated, by rupturing a diaphragm. First a diaphragm was placed between two areas which could be isolated (in terms of their pressures) from each other. Then, the diaphragm was forced to fail by increasing the pressure in one area while keeping the pressure constant in the other. Figure 5.1 illustrates the way in which this was implemented.

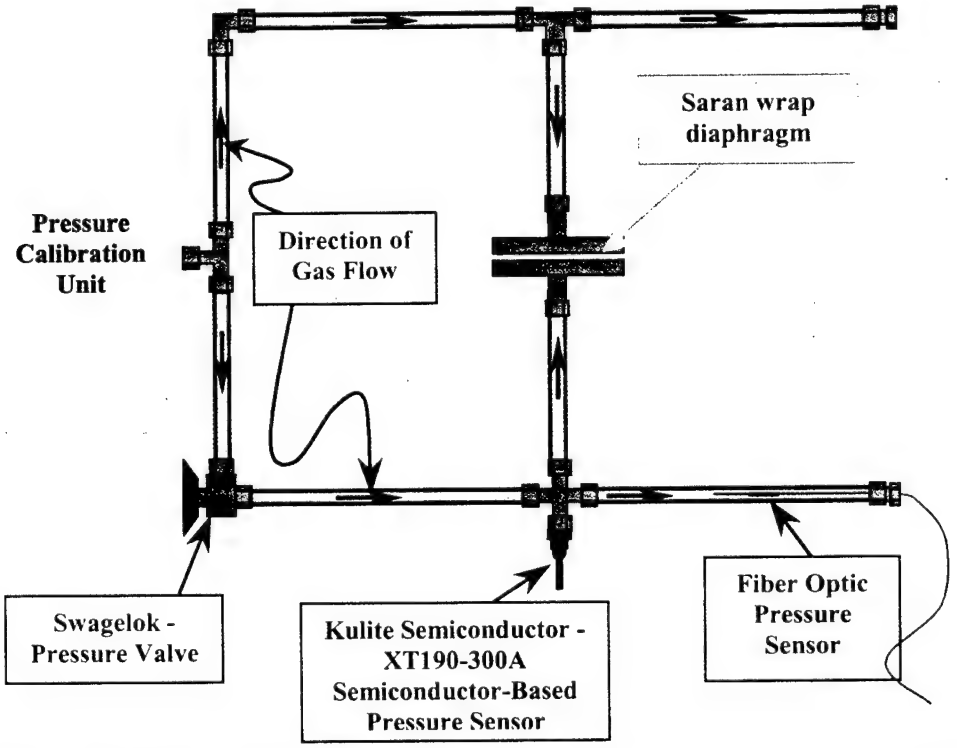

Figure 5.1: Schematic block diagram of the pressure chamber design. This was constructed using ¼ " stainless steel tubing, Swagelok™ fittings and Kurt J. Lesker Co. conflats.

The pressure calibration unit (Pressure Systems model# 9035) generates pressure in the system using purified nitrogen gas. The gas was pumped through the stainless steel tubing until the pressure inside the system reached 100 psi. At this point the valve was closed, isolating the pressure sensors from the pressure calibration unit. Then the pressure was increased at a slow but constant rate until the diaphragm, which was being held between two conflats, ruptured. Having carefully selected the material, the desired instantaneous change in pressure was achieved.

A photograph of this experiment is shown in Figure 5.2. The stainless steel tubing with the conflats attached, the semiconductor-based sensor, and the pressure calibration unit can be seen here. The optical fiber sensor cannot be seen at this resolution, but an arrow has been added to the diagram to label its position.

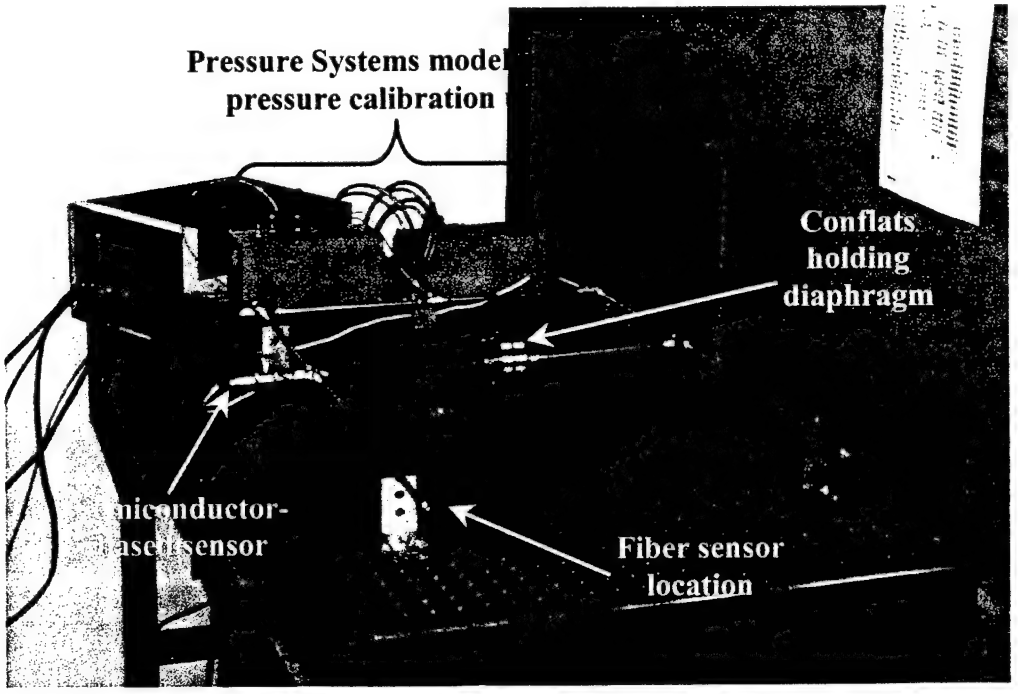

Figure 5.2: Photograph of the experimental setup. Labeled here are the pressure calibration unit, the conflats, the semiconductor-based sensor, and the fiber sensor.

To show that the experiment worked as designed, the experiment was performed and data was collected from the semiconductor-based sensor (see Section 6.3).

5.2 Pressure System Software

The DOS-based software provided with the pressure calibration unit prevented any other software from running simultaneously. National Instruments' LABView was chosen to implement another version of this application, which could be run along with the data acquisition software. A screen capture of the software is given in Figure 4.3 and the diagram for this *.vi can be found in Appendix C.

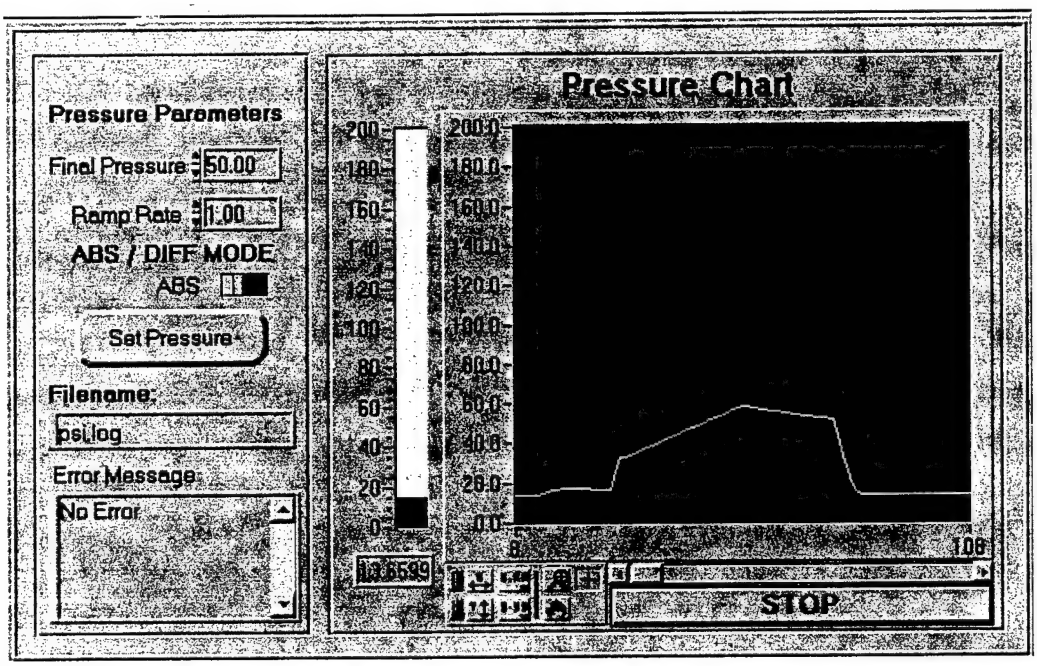

Figure 5.3: Screen capture of the pressure control unit LABView graphical user interface

This software makes it possible to instantaneously set or remove a pressure, or vary the pressure linearly. The system is able to hold the pressure constant to within 0.01 psi, and (most importantly) the system can run while the data acquisition software is running.

To operate this program, begin by typing a filename in the corresponding window, to let the program know where to store the values of pressure. Then press the run icon located in the toolbar of the LABView window to begin reading the pressure. Once running the program will be in one of three modes; set pressure, maintain pressure, and remove pressure. A description of each mode of operation and how to initiate it is listed below.

Table 5.1: Modes of Operation of the pressure control unit software

Mode	How to initiate mode	Program response
Set Pressure	- Key in or use the arrows to enter "Final Pressure". - Select a ramp rate (for instantaneous change make ramp rate about ¼ the "Final Pressure") - Press "Set Pressure" button	- A 5-10 sec pause will occur while – variables in the program are being initialized. - The pressure will jump to about 20 psi. - The pressure will increase at the rate specified to the final pressure.
Maintain Pressure	Allow set pressure operation to be executed.	The system will maintain a pressure within 0.01 psi of "Final Pressure"
Remove Pressure	1. Press the "Pressure Off" button. **OR** 2. Press the "STOP" button.	1. After a 1-2 sec pause the system will exponentially decay to the pressure in the room, without exiting the program. 2. Same as 1., except the program will stop running.

Note: Upon initiating the "Set Pressure" command, there is a delay before the pressure changes from the initial reading (pressure in the room). This is caused by the algorithm utilized in the software and can be easily eliminated given the time to investigate the exact source.

6. Preliminary Results

6.1 Design Results

A MATLAB function and the accompanying script file were developed to calculate the gage length and possible airgap values of the sensor. These have been attached in Appendix A. A few of the results of the design software were compared to sensors that have been used in the lab previously and the results of this are presented in Table 6.1 below.

Table 6.1: Comparison of experimental results and the sensor design program.

Design Parameters	Sensor Design No.							
	1		2		3		4	
	Design	Actual	Design	Actual	Design	Actual	Design	Actual
Measurement Range [psi]	7000	7000	4000	4000	2000	2000	900	900

It can be seen from the above data that the MATLAB code developed does not match the experimental results well. It was later determined that for the sensors presented as "Actual" the linear range was defined from 10% less than the maximum value of the sinusoidal component of the intensity to 10% more than the minimum. However, in the MATLAB code, the linear range is defined from 40% less than the maximum value of the sinusoidal component of the intensity to 40% more than the minimum. Intuitively it makes sense that this should result in the gage length being shorter in the design and after modifying the code to account for this, the designs in Table 6.2 were obtained.

Table 6.2: Comparison of experimental results the modified sensor design program.

Design Parameters	Sensor Design No.							
	1		2		3		4	
	Design	Actual	Design	Actual	Design	Actual	Design	Actual
Measurement Range [psi]	7000	7000	4000	4000	2000	2000	900	900

It can be seen here that the results obtained for designs 1, 2 and 4 match the actual gage length more closely than in the first model. However, it is also seen here that the sensor design 3,

grew less accurate. Upon further investigation, it was determined that the term "linear range" was defined differently in the past. Therefore the actual linear range of this sensor matched the definition of the first model.

6.2 Comparison of Intensity-Based and SCIIB Fiber Sensors

A comparison of the stability obtained by switching to SCIIB from an intensity-based system is presented in Figure 6.1.

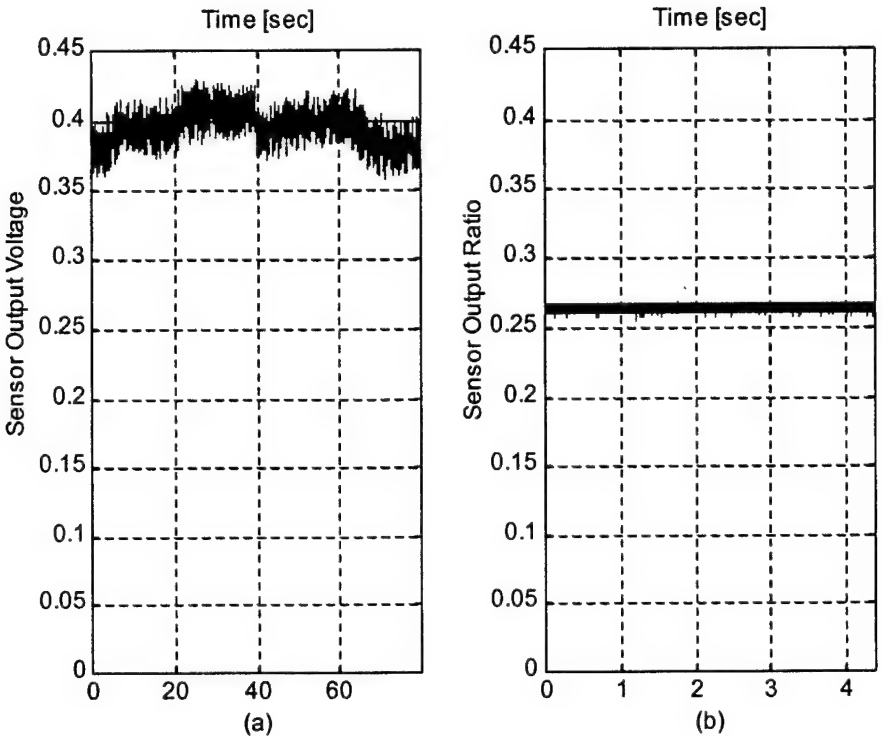

Figure 6.1: Comparison of the stability obtained by switching to SCIIB system. (a) Sensor output at 60 psi, using a tunable laser as a source in an intensity-based system. (b) Sensor output at 60 psi, using an SCIIB system.

Shown here is the output of the same sensor when connected to two different systems. This was performed at room temperature and in both cases data was collected with the system pressure at a constant 60 psi. By collecting data at different pressures within the operation range of the sensor, it was possible to obtain a calibration curve. This curve would later be used to determine the pressure from the measured output voltage. In this case, data was collected for a few seconds, until a few hundred kilobytes of data was stored (the amount of data captured not be controlled precisely because the sample rate was 12.5 kHz).

The error obtained by using the intensity-based system was about ± 0.1V, which corresponded

to ± 15 psi, while the SCIIB system demonstrated a variation of ± 0.08V or ± 2 psi. This sensor was actually designed for the 1550 nm source used in the intensity-based system and the SCIIB system used had a center wavelength of 1310 nm (hence the sensor was not in its optimum linear region). Therefore if it is assumed that the same voltage deviation exists when the correct sensor is used, it is possible to obtain a higher pressure-resolution.

6.3 Trial of the Experiment

As mentioned in Section 5.1, the experiment was performed and data was collected using the Kulite sensor. The experimental procedure is explained in detail below, however it was determined that the diaphragm ruptured as required using a similar method. The pressure was increased to a constant value of 25 psi and then the vale was closed. After that the pressure was further increased to generate the rupture of the diaphragm and thereby generate the desired instantaneous pressure change. Figure 6.2 shows the results obtained by performing this series of steps.

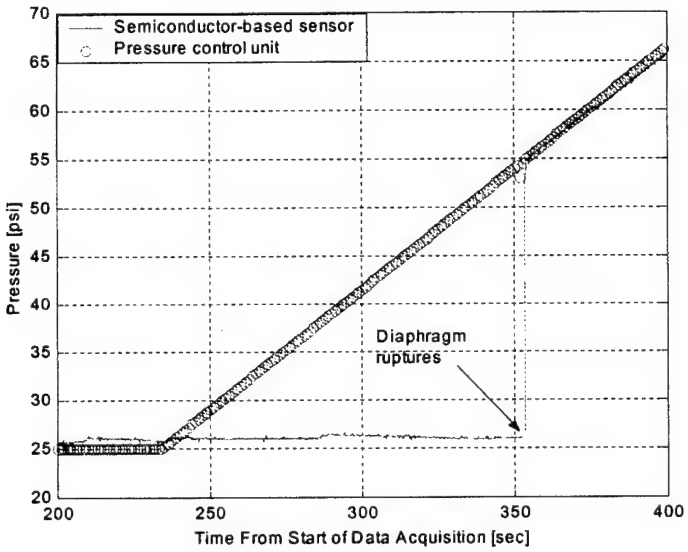

Figure 6.2: Data collected to verify that the pressure system worked as designed.

As shown in the diagram above, when the pressure difference between the two chambers is about 30 psi, the diaphragm ruptures and an *instantaneous* change in pressure is obtained. This was the desired effect, therefore it was concluded that the system design matched the actual performance closely.

Furthermore, to determine if there were any failures in the diaphragm prior to the rupture, which could cause leakage problems at higher pressures, the diaphragm was examined after the experiment. A single hole, with a diameter approximately equivalent to the inner diameter of the stainless steel tubing used in the experiment, was found in the diaphragm. No stretch marks or other signs of strain were found on the material, so the system was expected to operate at higher pressures. Figure 6.3 is a photograph of the diaphragm removed from between the conflats.

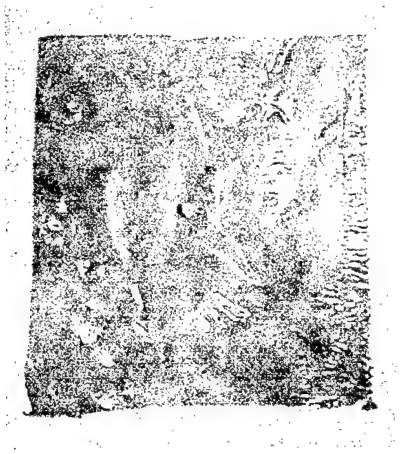

Figure 6.3: Photograph of a ruptured diaphragm. The hole in the center is the point of failure, and it is the diameter of the inner diameter of the stainless steel tubing used in the experiment.

7. Experiment

7.1 Pressure System

7.1.1 System Setup

The pressure control unit, the stainless steel tubing, the Swagelok™ fittings and the conflats were assembled as shown in Figure 5.2. Next, a new diaphragm was placed between the conflats in the pressure system (*The material chosen was plastic film (more commonly known as "Saran™ wrap"), because of its low cost, and because the pressure difference which causes it to rupture, is fairly low*). The pressure unit was connected to a supply of purified nitrogen gas, and then the power was connected and turned on. Then the LABView program was initialized and run to commence the data acquisition from the Pressure Systems 9035 pressure calibration unit.

7.1.2 Procedure

Using the software, the pressure was increased to 100 psi and was allowed to reach its "steady-state" operating point. The valve was then closed, and the pressure was further increased to 150 psi, at a rate of 0.25 psi/sec (unless otherwise stated). Data from the sensor(s) was recorded as mentioned in Section 7.2 below and it was determined that this system worked as originally intended.

7.2 Sensor System

7.2.1 System Setup

An SCIIB optical fiber sensor was fabricated by following the procedure explained in Section 4. The fiber sensor was then fed through a 1mm diameter hole, which had been previously drilled through a *cap* (Swagelok™ part description) and secured in place with epoxy. Aftyer the epoxy cured, this was physically connected to the pressure system by screwing the cap into the female fitting at the end of the tubing (Figure 5.1 or 5.2). The fiber was spliced to the SCIIB system being used, and the output channels of this system were connected to a data acquisition board capable of a maximum sampling rate of 100kHz. Power was connected and the SCIIB system was turned on.

The semiconductor-based sensor was physically connected to the pressure system using a stainless steel adapter. The power supply leads of the sensor were connected to a Tektronix

PS-503-A DC power supply and the signal leads were connected to the data acquisition board. The DC power supply was set to an output voltage of 10 V and then turned on.

7.2.2 Procedure

This output voltage data was stored for later processing using an ADAC 5404HDR data acquisition board and a program developed using LABView (Section 7.4).

7.3 Calibration

Calibration was required for the SCIIB optical fiber sensor in order to determine the mapping of the output voltage to an absolute value of pressure, and thereby determine the sensor's linear region of operation. The way in which this was performed was the sensor would be subjected to a constant pressure generated by the pressure calibration unit. The output voltage data would then be stored for a period of time using the data acquisition board (Section 7.4) and this operation would be repeated for several values of pressure. The data in each voltage output data file would then be averaged, and mapped to the actual pressure. This was used to generate a "calibration curve" (Section 8), which could be used to map the sensor output voltages under dynamic conditions to the actual pressure in the chamber.

7.4 Data Acquisition

The data acquisition board makes use of an integrated circuit called an analog-to-digital converter (ADC) to return the value of an analog signal at a specified time interval. Essentially this translates to taking an analog input and generating a digital output. The selected ADC was an ADAC 5404HDR board, capable of a maximum sampling frequency of 100kHz, which is the inverse of the "time interval" previously mentioned. When only one input is connected, this means that the ADC will return the value of this input signal every 10 μsec. However, when multiple channels are connected, the ADC shares the sampling capacity, and returns a value for each of the n input signals every n x 10 μsec.

A LABView program to perform this sampling was developed based on an example *.vi which accompanied the library files downloaded from ADAC's website (http://www.adac.com/). The front panel of the data acquisition program is show in Figure 7.1 below and the program diagram is present in Appendix C.

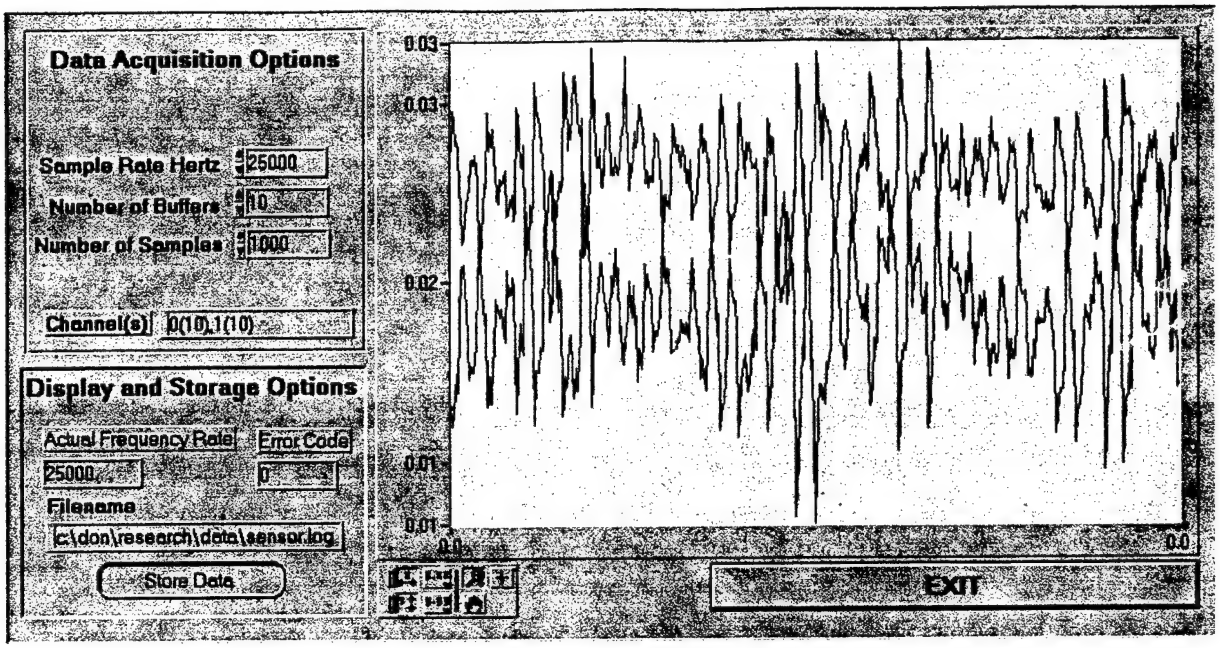

Figure 7.1: Screen capture of the data acquisition LABView graphical user interface

The setup described in Section 7.2 requires that three signals be connected to the data acquisition software and hence reducing the maximum sampling frequency by a third on each channel. Furthermore, it was realized that this data acquisition software could not achieve the stated maximum sampling frequency, unless there was no other software running. Since the pressure control software needed to run simultaneously, the maximum processing speed of the card could not be utilized. For this reason, the semiconductor-based sensor was used only for the initial calibration phase of the experiment. Most of the results presented here do not contain the semiconductor-based sensor data.

7.5 Post-Processing

This is the process whereby the sensor voltage data was converted to pressure data, and then converted to a frequency domain representation for analysis. A block diagram of the processes undertaken to perform this is shown in Figure 7.2.

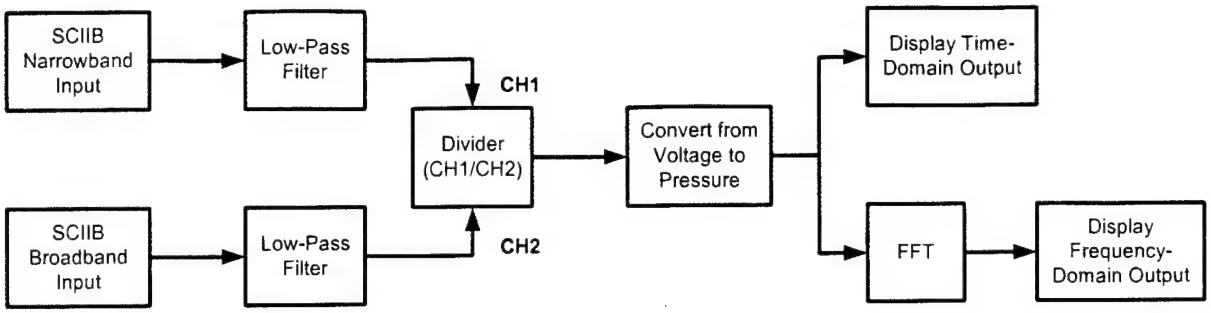

Figure 7.2: Block diagram of the DSP algorithm used to process the voltage output of the SCIIB system

First the file generated by the data acquisition board is divided into the narrowband and broadband channels. Each set of data is then passed through a finite impulse response (FIR) low pass filter and then the resulting data samples from the narrowband channel are divided by the samples from the broadband channel. The result is then mapped to a voltage using the calibration curve generated by following the steps laid out in Section 7.3. By taking the average of the samples (Section 7.3) and performing the same operation described in this paragraph, it was possible to generate the calibration curve. Therefore, the calibration data and the experimental data match as closely as possible. After this conversion takes place it is possible to analyze the data for how well it tracks the applied pressure (time domain analysis) and check the data for the frequency content (frequency domain analysis).

This is the process which was used to obtain the data presented in Section 8 of this paper. Figure 7.2 was implemented using MATLAB and the code for this can be found in Appendix D.

7.5.1 Low-Pass Filter Design Considerations

The low-pass filter at the output of the SCIIB unit is mainly to reduce out of band noise, and the main concern in designing this, is introducing distortion. Distortion of the voltage signal will lead to the values of pressure being incorrectly encoded. For this reason, a simple averaging filter with a length which could be selected by the user (i.e. MATLAB simulation software user) and varied depending on the signal-to-noise ratio (SNR) of the sensor output voltage.

7.5.2 Frequency Response Considerations

The initial idea was to determine the frequency response of the sensor from the Fourier transform of the burst data. The figure below shows the sensor output would ideally look like if an instantaneous change in pressure (i.e. it takes 0 seconds to change the pressure to switch from one value to the next) is generated and is measured by two sensors.

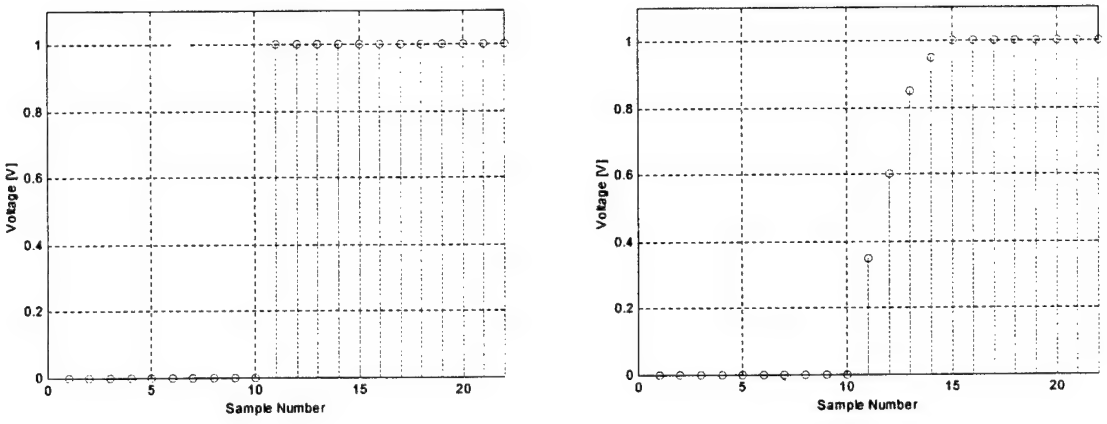

(a) (b)

Figure 7.3: Sampled sensor output for noiseless cases. (a) A sensor with a higher response time than the data acquisition board. (b) A sensor with a response which can be detected by the data acquisition board.

Assuming the output voltage of the sensor is sampled at the same rate in each case, the sensor in Figure 7.3 (a) has a higher frequency response. That is to say that this sensor adjusts to the pressure as quickly as the voltage signal can be sample. The sensor represented in Figure 7.3 (b) however, demonstrates a gradual rise to the final output voltage. This sensor has a lower frequency response and this can be demonstrated in the frequency domain as shown in Figure 7.4.

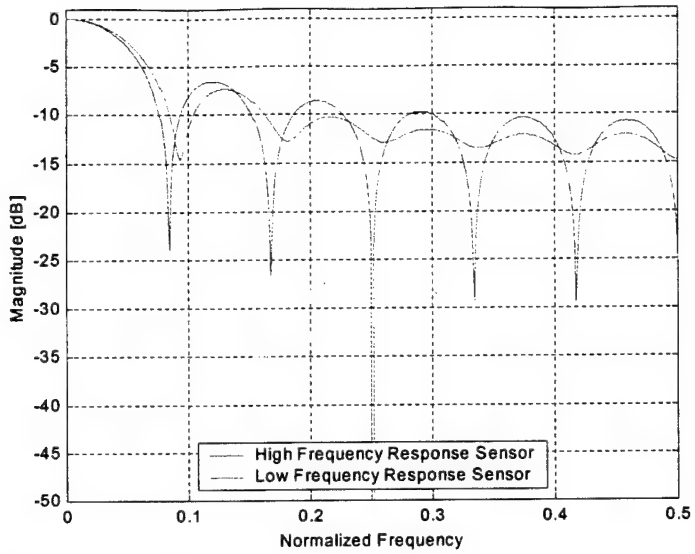

Figure 7.4: Frequency domain analysis of the sensor output voltage.

Shown in this figure, are the frequency domain representation of the high-frequency sensor output voltage and the low-frequency sensor output voltage on the same axes. It is easy to determine that the sensor with the lower frequency response can be characterized as such, because the high frequency content of the signal is attenuated in comparison with the transform of the other sensor data. However, quantifying the sensor frequency response in this manner would not be possible, without the benefit of sensor data from sensors with known frequency response and a developed model.

For this reason, the sensor frequency response was determined by measuring the time taken for the sensor to be deflected by 5 psi (the high frequency pressure component to be measured), or by interpolating this value from the data obtained. The reciprocal of this value would then be defined as twice the frequency response based on the Nyquist theorem.

8. Results

Using the method of sensor fabrication presented in the previous sections, two sensors having the parameters listed in Table 8.1 were used.

Table 8.1: Sensor Parameters

Parameters	Sensor #1	Sensor #2
Gage Length [mm]	9	9
Airgap [μm]	18.59	20.49
Tube Outer Diameter [μm]	270	220
Anticipated Linear Range [psi]	310	259
Anticipated Frequency Response [kHz]	94.5	90.3

Once placed in the system, sensor #1 proved too insensitive to the pressure variations being generated, therefore the results presented here are solely from sensor #2. These parameters were tested according to the experimental procedures laid out in Section 7 at room temperature and at 300 °F.

8.1 Room-Temperature Experimental Results

First, as mentioned in section 7.3, a calibration curve was generated in order to determine the pressure measured by the sensor. The curve will ideally be a linear plot (i.e. the sensor is in its linear operating range over all values of applied pressure), but the curve for this sensor turned out to be best approximated using a 3rd order polynomial.

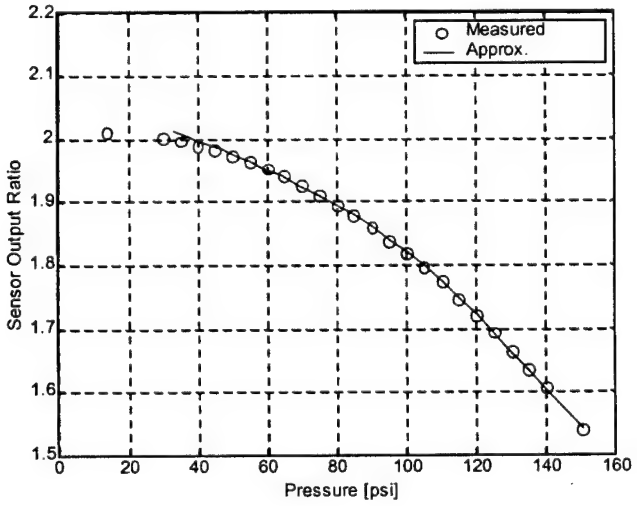

Figure 8.1: Room temperature pressure calibration curve.

It can be seen in this figure that the voltage does not correspond to the values of pressure linearly over the entire range of measured pressures. Therefore the voltage measurements at or above 2.00 V will have to be discarded, since the sensor output voltage will not vary much with change in applied pressure.

This relationship was then used to map the voltages to the actual pressure after the experiment was performed. The result from performing this experiment at room temperature is shown in the figure below.

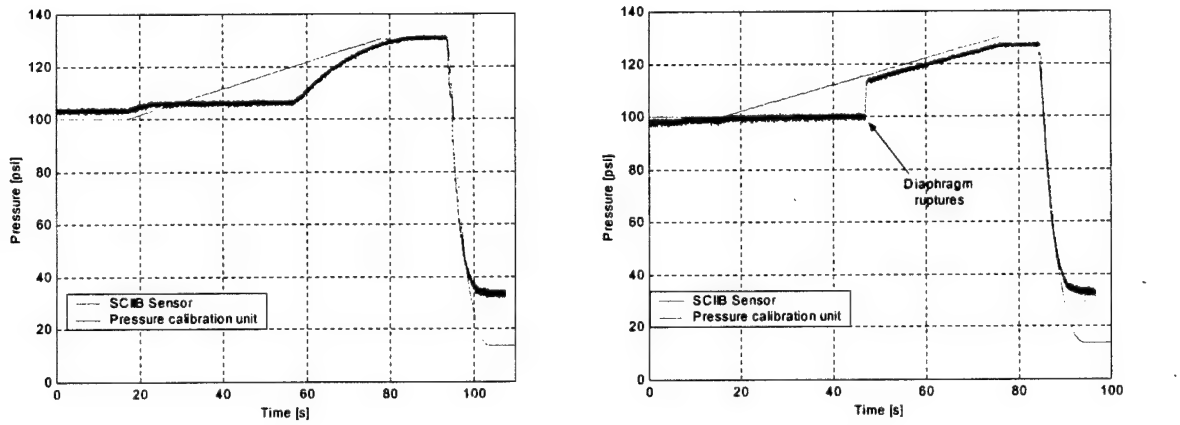

Figure 8.2: Room temperature SCIIB optical fiber sensor output and the pressure calibration unit data plotted on the same axes. (a) Trial #1: the diaphragm material developed a slow leak. (b) Trial #2: the diaphragm once again ruptured as desired.

Figure 8.2 (a) was the first trial of the sensor at room temperature and as can be seen here an unexpected result was obtained. It turned out that diaphragm material failed by rupturing slowly. This was most likely due to inconsistencies in the plastic material used as the diaphragm. However in Figure 8.2 (b), it can be seen that the sensor behaved as anticipated. An instantaneous change in pressure can be generated as and this was then analyzed for frequency content.

It was then necessary to determine the frequency response of the sensor. This was performed as described in Section 7.5.2. The results obtained show that when subjected to room temperature, the pressure sensor has a frequency response of 38.5 Hz.

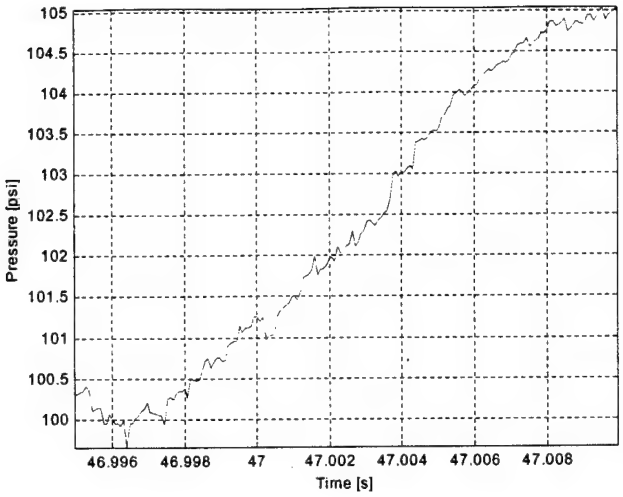

Figure 8.3: Close up view of the output voltage at the time of the rupture. This was used to determine the sensor frequency response.

Note: Room temperature at the time these measurements were taken was about 71 °F.

8.2 High-Temperature Experimental Results

The heating tape was then wrapped around outside the stainless steel tubing in the location of the SCIIB sensor, to generate higher temperatures inside the chamber. Since the cap had already been bonded with the fibers, the thermocouple had to be placed on the outside of the tubing. In order to determine the temperature being experienced by the sensor, the cap with the fibers through it was removed and the thermocouple was placed down the tube to the location where the sensor would be found. A cap was then placed at the open end of the tubing and the temperature inside was measured after the system was heated to a known temperature and allowed to settle at a constant temperature. The results of this are presented in Table 8.2.

Table 8.2: Comparison of temperature inside the chamber to reading from the outside

OUTSIDE TEMPERATURE READING [°F]	INSIDE TEMPERATURE READING [°F]
72	72
200	195
300	280
500	470

8.2.1 Results at 300 °F

This experiment was then carried out again at 300 °F. First, a calibration curve was generated and it can be seen here that the sensor is not in its linear operating region over the 0 to 150 psi range. As a result, any voltage reading above 1.95 V could have one of two values. Therefore, all readings lower than about 55 psi are going to be ignored for the discussion.

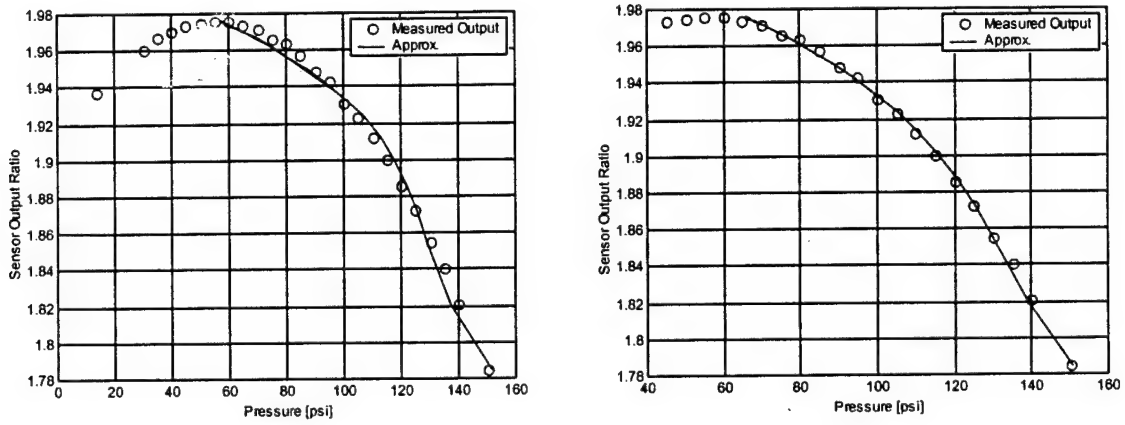

Figure 8.4: Calibration curves for the sensor with the 220 μm outer diameter at 300 °F outer temperature. (a) Initial calibration curve which included all points on the anticipated linear measurement range. (b) Calibration curve used to increase the accuracy over the range 80 psi to 150 psi.

The most obvious feature of the calibration curve after the sensor has been exposed to the high temperature environment for an extended period of time (about 1.5 hours to perform the test), is that its linear region of operation has been significantly reduced. After discarding the first 4 data points and performing generating a new calibration curve, it turned out that only the data from 90 psi to 150 psi could be trusted. This was because voltage information corresponding to the other values of pressure would be ambiguous, and therefore the pressure data would be unreliable.

Figure 8.5 below shows the data obtained after running the experiment as described in Section 7.

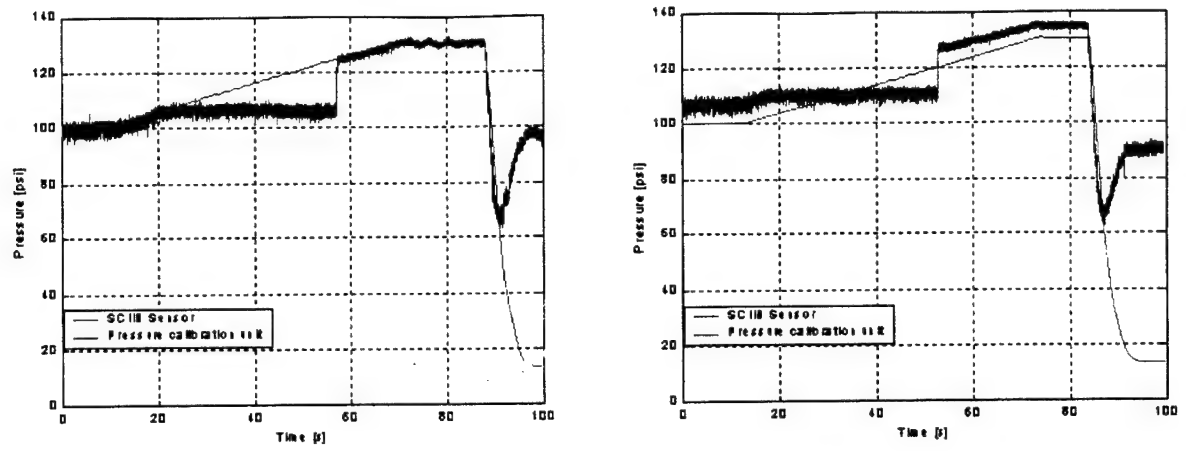

(a) (b)

Figure 8.5: SCIIB optical fiber sensor output at 300 °F plotted together with the pressure calibration unit data. (a) Trial #1: the data tracks the calibration unit data well, even the unstable section of pressure generation. (b) Trial #2: the data is shifted, but the experiment worked. The shift is possibly a by-product of the temperature drift of the SCIIB system.

As expected, the data below 80 psi is incorrectly mapped to higher values of pressure. This neglected, both sets of data have trends which match the pressure calibration unit's pressure reading. This means that the sensor works and can give pressure readings over the dynamic range required (100 psi ±5 psi). However, the data in the second trial did not match the curve exactly and this provided some concern about the repeatability of the sensor output. For this reason, the sensor was tested again when the system cooled down to see if it could still be used with the calibration curve of Section 8.1. Figure 8.6 shows the result.

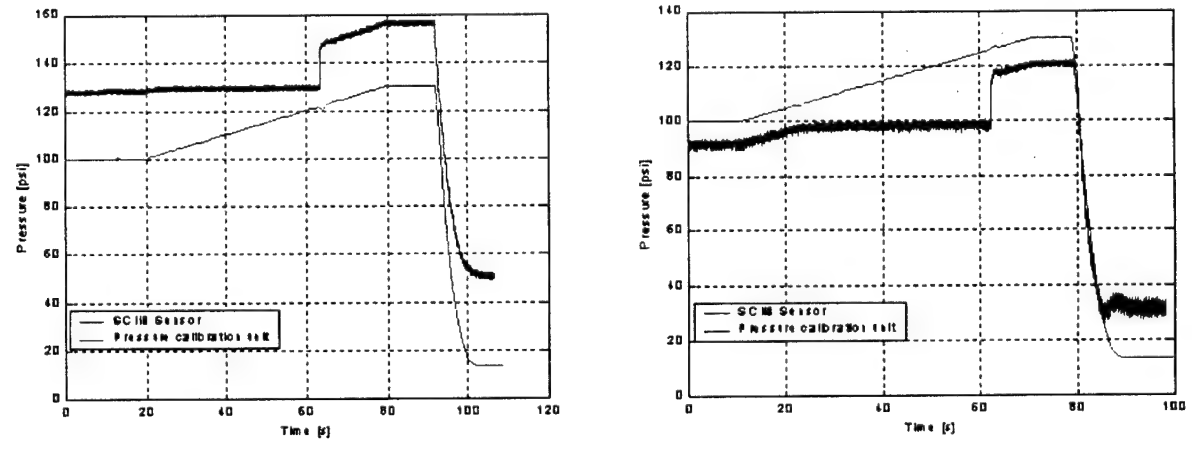

(a) (b)

Figure 8.6: Room temperature sensor data generated using the calibration curve in Section 8.1. The system was cooled to room temperature after performing the measurements at 300 °F, and the experiment was performed after the system was allowed to cool for 30 minutes (a), and 12 hours (b).

The figure shows that once the sensor is heated and cooled again, a new calibration curve must be created. It is also important to note that the features of the SCIIB sensor output (such as the shape of the curve and the impulse in pressure where there is a disruption in the calibration unit measurement) are exactly as would be anticipated. The only true problem is that the sensor voltage is being mapped to the incorrect value of pressure.

The frequency response of the sensor was measured to be 31.3 Hz.

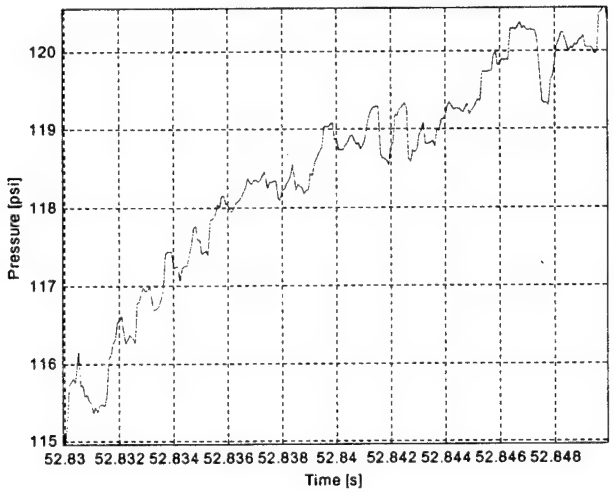

Figure 8.7: Close up view of the output voltage at the time of the rupture. This was used to determine the sensor frequency response.

8.2.2 Results at 500 °F

Once again the temperature was increased and measurements were taken to obtain the calibration curve presented in Figure 8.8. This shows that the system is linear over a similar range to the range obtained for the room temperature case.

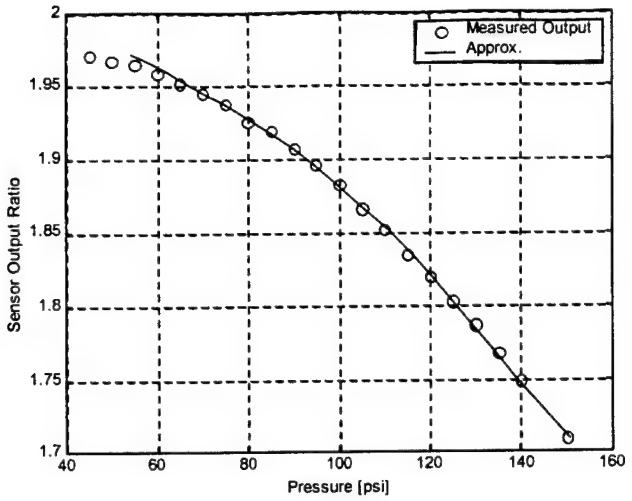

Figure 8.8: Calibration curve for the sensor with the 220 μm outer diameter at 500 °F outer temperature.

The experiment was then carried out as explained in previous sections and the results are shown in the figure below.

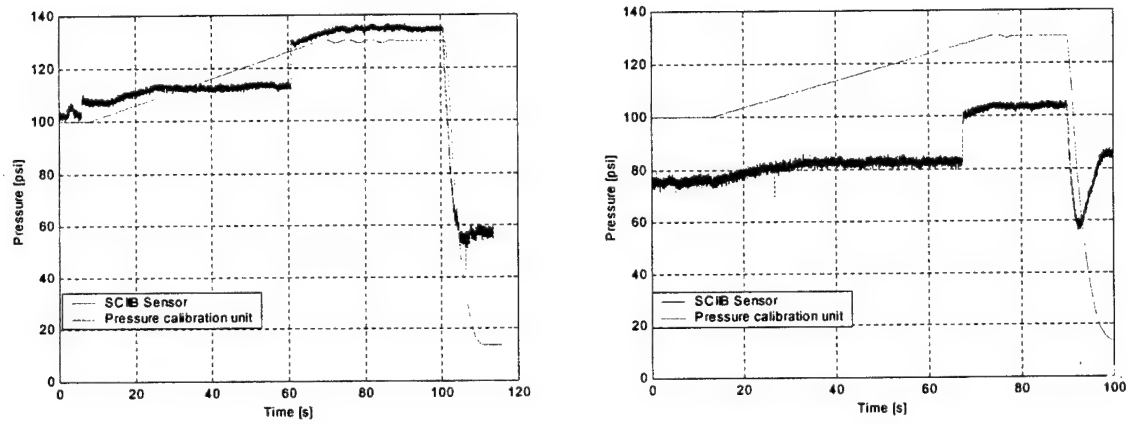

Figure 8.9: Two trials o f the SCIIB optical fiber sensor output at 500 °F plotted together with the corresponding pressure calibration unit data.

The data in the first trial did not match the pressure calibration unit very accurately, however it showed better performance than in the second trial. The data is incorrect because the calibration curve no longer represents the SCIIB calibration curve generated previously. It takes roughly 30 minutes to perform the experiment, which means that either the sensor's properties or the SCIIB unit's properties change during this time period. Further testing must be done to verify which.

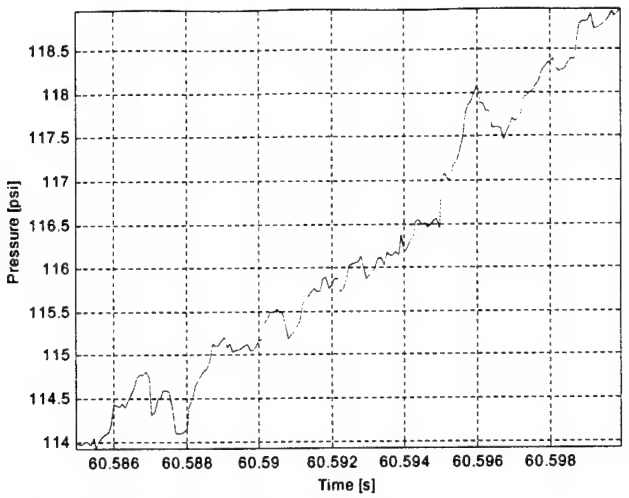

Figure 8.10: Close up view of the output voltage at the time of the rupture.

The frequency response of the sensor at 500 °F was determined to be 33.3 Hz, which means that the sensor frequency response is fairly constant over the entire temperature range measured.

8.3 Sensor Resolution

The resolution of the sensor was determined by finding the standard deviation of the output voltage at different values of pressure. This would give the voltage fluctuation and can be matched to the pressure fluctuation by using the calibration curve. The standard deviation is listed in Table 8.3 and Table 8.4.

Table 8.3: Standard deviation of the sensor output for room temperature measurements

PRESSURE [PSI]	VOLTAGE STANDARD DEVIATION [V]	PRESSURE STANDARD DEVIATION [PSI]
30	0.0021	1.0
50	0.0019	0.8
70	0.0020	0.7
90	0.0017	0.5
110	0.0017	0.3
130	0.0014	0.2
150	0.0012	0.2
AVERAGE		0.5

Table 8.4: Standard deviation of the sensor output for high temperature measurements

PRESSURE [PSI]	VOLTAGE STANDARD DEVIATION [V]	PRESSURE STANDARD DEVIATION [PSI]
30	0.0019	N/A
50	0.0018	N/A
70	0.0016	1.5
90	0.0015	1.1
110	0.0020	0.5
130	0.0013	0.3
150	0.0013	0.5
AVERAGE		0.8

By this method of analysis, the resolution of this sensor is the one order of magnitude shy of the requirement, because for the high-temperature the resolution is about 0.8 psi.

This resolution was significantly improved when it was discovered that one of the two boxes that comprises the pressure calibration unit was not grounded properly. The figure below shows the results when the experiment was performed again with the improved resolution. The noise was reduced by a factor of 10, but further analysis has not been performed to date.

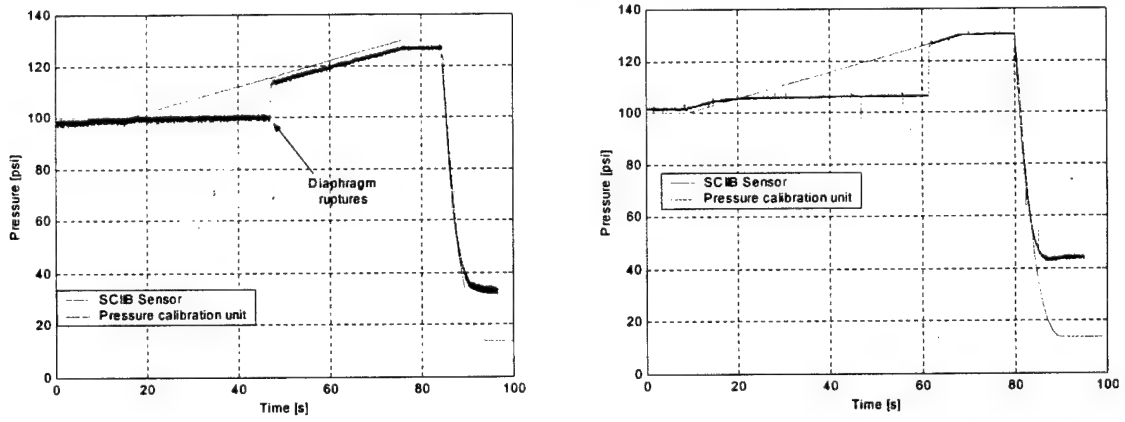

Figure 8.11: Plots demonstrating the improvement once the noise was isolated. (a) Sensor output before the pressure calibration unit was grounded. (b) Sensor output after the pressure calibration unit was properly grounded.

8.4 Temperature Effects

It had previously been stated that the SCIIB sensor is highly temperature insensitive. Therefore it was necessary to ensure that the modification to the sensor did not compromise this desirable feature of the sensor. The sensor was cooled from 300 °F to room temperature

while the sensor was exposed to normal atmospheric pressure. The voltage output of the sensor is shown in Figure 8.8.

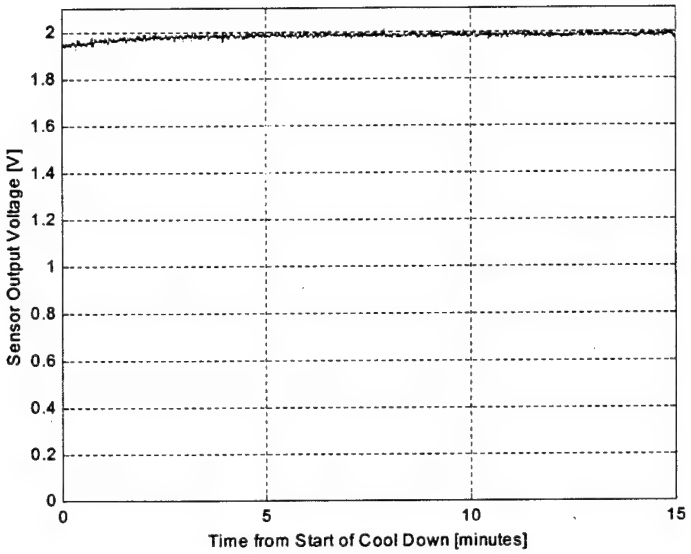

Figure 8.12: Voltage output of the SCIIB sensor when the temperature is decreased from 300 °F, to room temperature.

This could not be directly converted to a pressure reading with the calibration curve since the value of voltage exceeded the maximum reliable value of 1.95V (Section 8.2). However, the temperature-induced change in voltage was about 40 mV, which would correspond to about 10 psi based on the calibration curve. It is believed that by making the sensor as thin as this one, the temperature sensitivity has been increased.

9. Conclusion and Suggestions for Future Work

9.1 Conclusion

Table 9.1 is a summary of the sensor requirements and how these compare to the sensor used to obtain the above data.

Table 9.1: Summary of the targets and the results obtained

PARAMETER	SPECIFICATION	
	DESIRED	ACTUAL
Maximum pressure to be measured	150 psi	150 psi
High-frequency pressure component	5 psi	5 psi
Maximum temperature to withstand	500 °F	470 °F
Desired resolution	0.1% ≈ 0.1psi	0.8
Desired sensor frequency response	150kHz	30 Hz (average)

From the table above it can be seen that the requirements are yet to be met. The sensor system currently needs to have a significant improvement in its frequency response. However, the sensor resolution was improved after the discovery and isolation of a major contributor to the overall system noise. The resolution will be further improved from 0.8 psi, and may even meet the design specifications.

The SCIIB sensor is a viable solution to the problem of measuring pressure in a gas turbine engine. The modifications in the sensor design had the designed effect, but due to additional undesirable effects, the sensor turned out to be too fragile to implement. Also, a frequency response of 38.5 Hz was demonstrated using an analog SCIIB sensor system at 1310 nm, but this response was limited by the analog system. There was a 1 kHz low pass filter on the narrow-band channel and the output was then passed through the post-processing filter of length 100. Therefore it will be necessary to change the analog electronics in the SCIIB unit to support high frequency changes in the sensor signal, as well as performing the improvements recommended in the *Future Work* section of this paper.

Apart from this, programs were developed to control a pressure calibration unit, and a data acquisition board, and MATLAB code was implemented to design the sensor and to perform processing on the output data. It was determined that this code does not work well for the

sensors described here. The model stated higher frequency response curves that were a few orders of magnitude different from the measured values.

9.2 Suggestions for Future Work

The structure of the sensor should be modified. There are a few reasons for this, including:

1. It will be preferred that the sensor is flush-mounted in the engine. The current design makes this very difficult.
2. The design mentioned here makes the sensor more sensitive, but less rugged. This fragility is undesirable in the gas turbine engine environment described in Section 1 of this paper.
3. Initial tests show an increased sensitivity to fluctuations in temperature, but further investigation is needed.

Also, the results were not repeatable, meaning that a calibration curve needed to be generated each time, prior to using the sensor. This is a serious concern and while it is possible that this is a result of the modification performed on the sensor, more research is needed here.

Finally, the trade-off between the sensor resolution and the frequency response may be characterized. These two variables are related and if an accurate model could be developed for these sensors, perhaps this structure will not have to be abandoned for its inability to produce the desired frequency response.

10. References

[1] A. Wang, H. Xaio, R.G. May, J. Wang, W. Zhao, J. Deng, P. Zhang and G.R. Pickrell; "Optical Fiber Sensors for Harsh Environments"; in *International Conference on Sensors and Control Techniques* (ICSC 2000), Desheng Jiang, Anbo Wang, Editors, Proceedings of SPIE Vol. 4077, pp. 2-6, Proc. SPIE Vol. 4077, (2000)

[2] Alan D. Kersey and Anthony Dandridge; "Applications of Fiber-Optic Sensors"; *IEEE Transactions on Components, Hybrids, and Manufacturing Technology*, vol. 13, no. 1, pp. 137-143, March 1990

[3] C. Belleville and G. Duplain; "White-Light Interferometric Multimode Fiber-Optic Strain Sensor"; *Optics Letters*, vol. 18, no. 1, January 1993.

[4] L. Fabry Perot; *Journal of Physics, Vol. 7, 1898*

[5] Hai Xiao; "*Self-Calibrated Interferometric / Intensity-Based Fiber Optic Pressure Sensors*"; Doctor of Philosophy Dissertation; August 2000; Virginia Polytechnic Institute and State University

[6] Anbo Wang, Hai Xaio, J. Wang, Zhiyong Wang, W. Zhao and R.G. May; "Self-Calibrated Interferometric–Intensity-Based Optical Fiber Sensors"; *Journal of Lightwave Technology*, vol. 19, no. 10, pp.1495-1501, October 2001

Appendix A:
MATLAB Code for Sensor Design

```
function [L, ag, lambda, p_max] = gage_ag(r_o,r_i,r_f,N);
%
%  This function returns the gage length
%  of a pressure sensor, given the design
%  parameters. This program will prompt
%  for the other values that it needs.
%
%  USAGE:  [L, ag, lambda, p_max] = gage_ag(r_o,r_i,r_f,N);
%
%      L : Length between bonding points
%          of the sensor
%     ag : Vector containing possible values
%          for the distance between the source
%          fiber and the reflecting fiber
% lambda : Wavelength of the source
%  p_max : Maximum pressure to be measured
%    r_o : outer radius of the tube
%    r_i : Inner radius of the tube
%    r_f : Fiber radius (with the
%          buffer removed)
%      N : Number of air gap values to
%          calculate

% Declare constants and obtain other
% parameters from the user
E1     = 10.5E6;
mu     = 0.17;
rho    = 2.201E6;
lambda = input('Wavelength of the source [nm]: ') * 1E-9;
p_max  = input('Maximum pressure [psi]: ');

% Calculate the maximum airgap change allowed
d_max = (lambda/(2*pi)) * asin(0.900);

% Calculate the gage length
R = ((r_o^2) - (r_i^2))/ (r_o^2);
L = d_max * (E1/p_max) * R * (1/(1 - (2 *mu)));


% Calculate the airgap
delta_d = (lambda/2) - (lambda/(4*pi))*acos(-0.6);
d_0     = 2 * delta_d + ((lambda/(4*pi)) * acos(-0.6));
for ctr = 1:2:N
   ag(ctr)   = d_0 + (ctr * lambda);
   ag(ctr+1) = d_0 + ((ctr+1) * lambda);
end
```

```
function freq = freq_resp(r_o,r_i,r_f,L,ag,ratio);
%
%  This function calculates the frequency
%  response of a tube constructed sensor.
%
%  USAGE: freq = freq_resp(r_o,r_i,r_f,L,ag,ratio);
%
%         freq : Frequency response of the
%                sensor
%          r_o : Outer radius of the tube
%          r_i : Inner radius of the tube
%          r_f : Fiber radius (with the
%                buffer removed)
%            L : Length between bonding
%                points of the sensor
%           ag : Distance between the source
%                fiber and the reflecting fiber
%        ratio : Ratio of 'length of reflecting
%                fiber/gage length'

% Declare variables
E2    = 7.24E10;
rho   = 2.201E6;

% Calculate the Frequency response
S_tube = pi * ((r_o^2) - (r_i^2));
V_tube = L * S_tube;
V_refl = pi * (r_f^2) * ((ratio * L) - (0.5 * ag));
freq   = (1/(2*pi)) * sqrt((S_tube * E2 * 1000) ...
   /(L * (V_tube + V_refl) * rho));

% To see where the extra factor of 1000 comes
% from, manipulate the units in the equation
```

```
clear all
close all
clc

% Declare constants and obtain other
% parameters from the user
o_d = input('Tube outer diameter [um]: ');
i_d = input('Tube inner diameter [um]: ');
f_d = input('Fiber outer diameter [um]: ');
clc
r_o = o_d*1E-6/2;
r_i = i_d*1E-6/2;
r_f = f_d*1E-6/2;
N   = 30;

% Calculate the gage length and the airgap
[L, ag, lambda, p_max] = gage_ag(r_o,r_i,r_f,N);

% Display the values of airgap for calculating the
% frequency response
disp(' ')
for ctr = 1:floor(N/2)
   disp([num2str(ctr) ' -  ' num2str(ag(ctr)) '     ' ...
         num2str(ctr+floor(N/2)) ' -   ' ...
         num2str(ag(ctr+floor(N/2)))]);
end

num = input('Which air gap will you use? [Index #]: ')
clc

% Calculate the Frequency response
ratio = 0.5;
freq  = freq_resp(r_o,r_i,r_f,L,ag(num),ratio);
clc

% Display the airgap
disp(' ');
disp('Values of airgap [um]:');
for ctr = 1:2:N
   disp([num2str(chop(ag(ctr)*1E6,5)) ' ' ...
      num2str(chop(ag(ctr+1)*1E6,5))]);
end

% Display the other results obtained
disp(' ');
disp(['Gage Length:      ' num2str(L*1E3) ' mm']);
disp(['Airgap:        ' num2str(ag(num)*1E6) ' um']);
disp(['Frequncy Response:  ' num2str(freq*1E-3) ' kHz']);
disp(' ');
```

Appendix B
LABView Block Diagram of Pressure Control Unit Program

PSI Control.vi
C:\Don\Research\Specialized Software\PSI Control.vi
Last modified on 11/29/01 at 1:17 PM
Printed on 11/30/01 at 10:52 PM

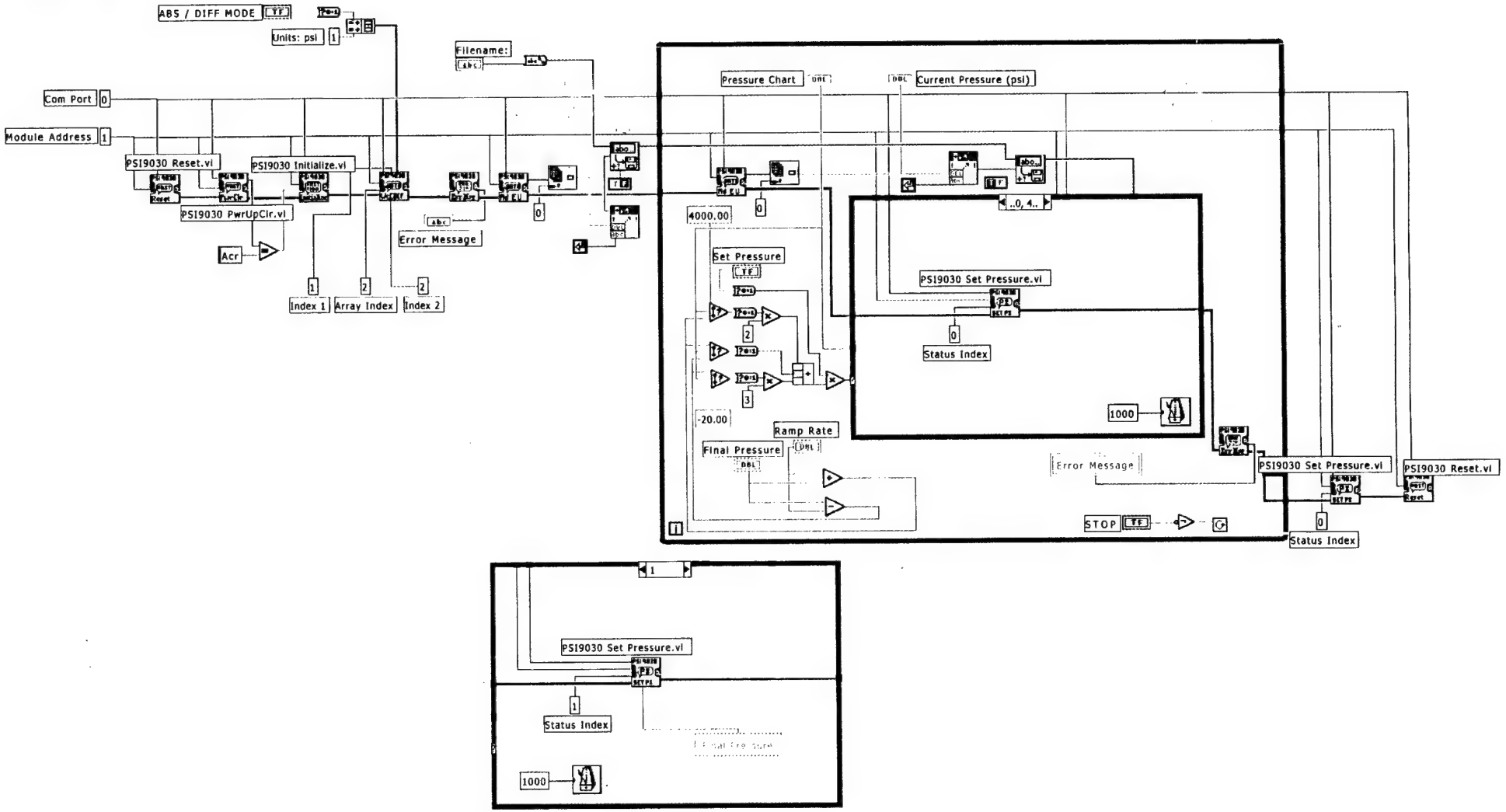

PSI Control.vi
C:\Don\Research\Specialized Software\PSI Control.vi
Last modified on 11/29/01 at 1:17 PM
Printed on 11/30/01 at 10:52 PM

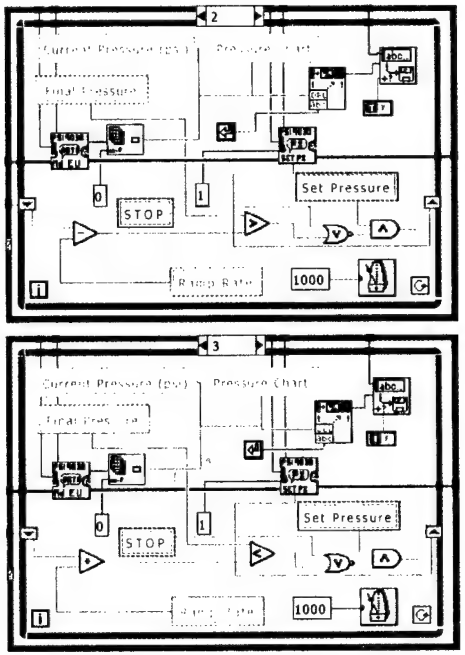

Appendix C:
LABView Block Diagram of Data Acquisition Program

ADAC ADQ II.vi
C:\Program Files\National Instruments\LabVIEW\AFOSR VIs\ADAC ADQ II.vi
Last modified on 11/29/01 at 2:04 PM
Printed on 12/12/01 at 2:00 PM

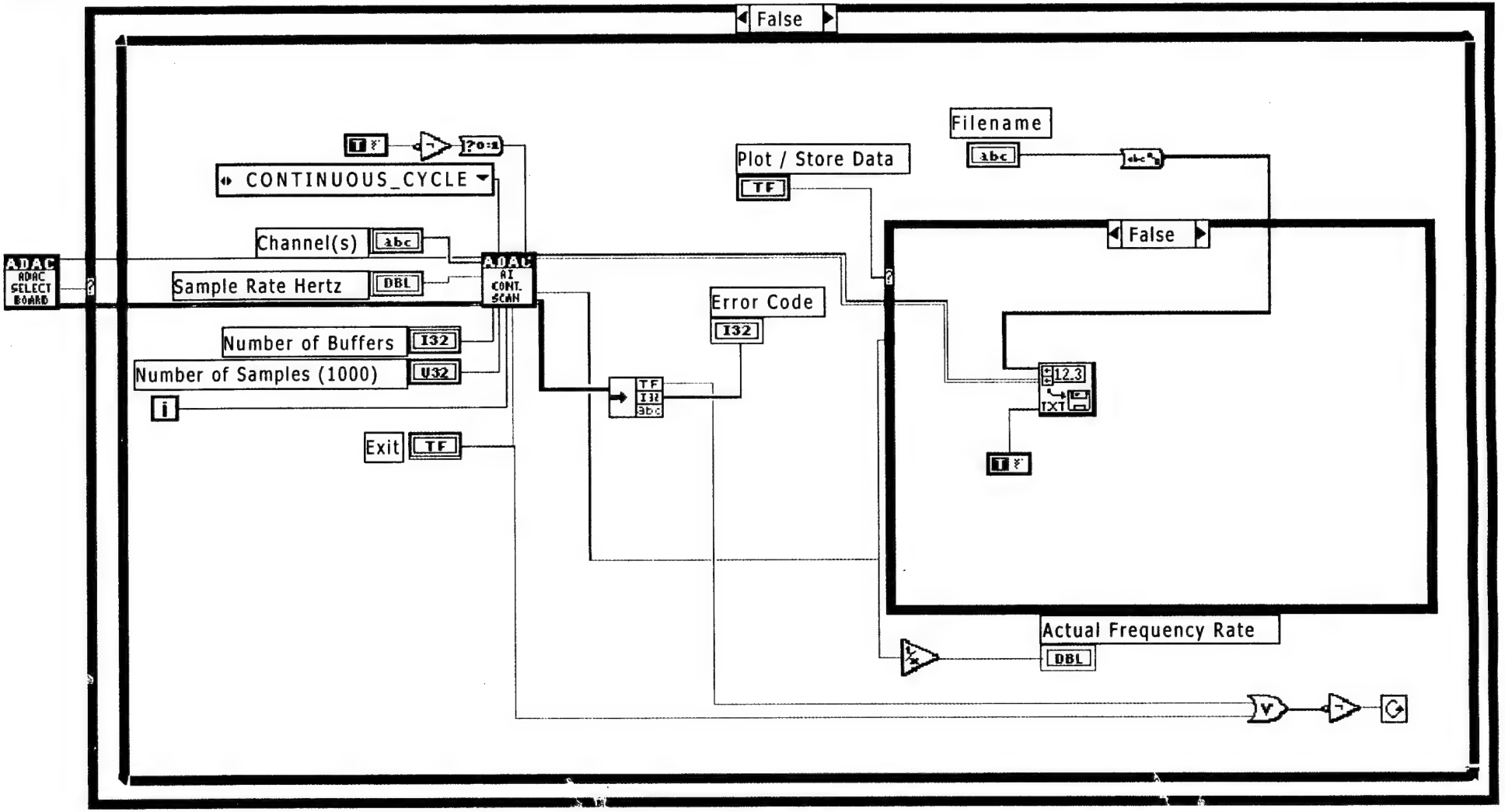

ADAC ADQ II.vi
C:\Program Files\National Instruments\LabVIEW\AFOSR VIs\ADAC ADQ II.vi
Last modified on 11/29/01 at 2:04 PM
Printed on 12/12/01 at 2:00 PM

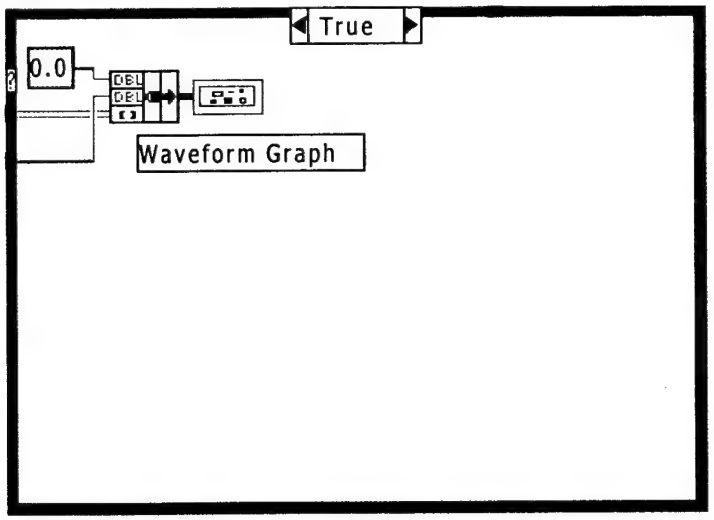

Appendix D:
MATLAB Code for Post-Processing Algorithm

```
function y = ave_filter(x, ave_num);
%
%  This function performs an averaging filter
%  operation using the 'mean' command. The
%  number of samples to be averaged is specified
%  by the user.
%
%
%  USAGE : y = ave_filter(x, ave_num);
%
%          y : Filtered output
%          x : Input signal to be filtered
%    ave_num : Number of samples to average
%
%
%  See also: MEAN

l1     = length(x);
x      = reshape(x,1,l1);
x      = [x(floor(ave_num/2):-1:2) x x(end:-1:end-floor(ave_num/2))];
l2     = length(x);
y      = zeros(1,l1);
y_temp = zeros(1,l2);

for ctr=1:l2-ave_num
   if ctr ==1
      y_temp(ctr) = mean(x(ctr:ctr+ave_num-1));
   else
      y_temp(ctr) = y_temp(ctr-1)+(x(ctr+ave_num-1)-x(ctr-1))/ave_num;
   end
end

y = y_temp(1:l1);
```

```
function p = calibrate(ord,filename,show_res);
%
%  This function returns the vector P
%  to be used by the command polyval
%  for an SCIIB sensor. This function
%  must be editted before it is used, in
%  order to verify that the actual files
%  match those listed here.
%
%
%  USAGE : p = calibrate(ord,filename,show_res);
%
%          p : Vector to be used in the
%              MATLAB's 'polyval' command
%        ord : Order of the polynomial that
%              data will be 'fit' to
%   filename : Name of file where 'p' is to be
%              stored
%   show_res : Display the calibration curve?
%              'y' or 'n'
%
%  See also: POLYFIT, POLYVAL

% Read the necessary data files
p01    = dlmread('013_6.log');
p02    = dlmread('030.log');
p03    = dlmread('035.log');
p04    = dlmread('040.log');
p05    = dlmread('045.log');
p06    = dlmread('050.log');
p07    = dlmread('055.log');
p08    = dlmread('060.log');
p09    = dlmread('065.log');
p10    = dlmread('070.log');
p11    = dlmread('075.log');
p12    = dlmread('080.log');
p13    = dlmread('085.log');
p14    = dlmread('090.log');
p15    = dlmread('095.log');
p16    = dlmread('100.log');
p17    = dlmread('105.log');
p18    = dlmread('110.log');
p19    = dlmread('115.log');
p20    = dlmread('120.log');
p21    = dlmread('125.log');
p22    = dlmread('130.log');
p23    = dlmread('135.log');
p24    = dlmread('140.log');
p25    = dlmread('150.log');

% Apply SCIIB to each data point
p_1    = (p01(1:2:end)./(p01(2:2:end)));
p_2    = (p02(1:2:end)./(p02(2:2:end)));
p_3    = (p03(1:2:end)./(p03(2:2:end)));
p_4    = (p04(1:2:end)./(p04(2:2:end)));
p_5    = (p05(1:2:end)./(p05(2:2:end)));
p_6    = (p06(1:2:end)./(p06(2:2:end)));
p_7    = (p07(1:2:end)./(p07(2:2:end)));
p_8    = (p08(1:2:end)./(p08(2:2:end)));
```

```
p_9     = (p09(1:2:end)./(p09(2:2:end)));
p_10    = (p10(1:2:end)./(p10(2:2:end)));
p_11    = (p11(1:2:end)./(p11(2:2:end)));
p_12    = (p12(1:2:end)./(p12(2:2:end)));
p_13    = (p13(1:2:end)./(p13(2:2:end)));
p_14    = (p14(1:2:end)./(p14(2:2:end)));
p_15    = (p15(1:2:end)./(p15(2:2:end)));
p_16    = (p16(1:2:end)./(p16(2:2:end)));
p_17    = (p17(1:2:end)./(p17(2:2:end)));
p_18    = (p18(1:2:end)./(p18(2:2:end)));
p_19    = (p19(1:2:end)./(p19(2:2:end)));
p_20    = (p20(1:2:end)./(p20(2:2:end)));
p_21    = (p21(1:2:end)./(p21(2:2:end)));
p_22    = (p22(1:2:end)./(p22(2:2:end)));
p_23    = (p23(1:2:end)./(p23(2:2:end)));
p_24    = (p24(1:2:end)./(p24(2:2:end)));
p_25    = (p25(1:2:end)./(p25(2:2:end)));

% Calculate the values for polyfit function
pm = [mean(p_1) mean(p_2) mean(p_3) mean(p_4) ...
      mean(p_5) mean(p_6) mean(p_7) mean(p_8) ...
      mean(p_9) mean(p_10) mean(p_11) mean(p_12) ...
      mean(p_13) mean(p_14) mean(p_15) mean(p_16) ...
      mean(p_17) mean(p_18) mean(p_19) mean(p_20) ...
      mean(p_21) mean(p_22) mean(p_23) mean(p_24) mean(p_25)];

pa = [13.7 30 35 40 45 50 55 60 65 70 75 80 85 90 95 100 105 110 ...
      115 120 125 130 135 140 150];


% Perform a best fit on the data
p = polyfit(pm(5:end),pa(5:end),ord);

% Display Calibration Curve
if show_res == 'y'
   y = polyval(p,pm);
   figure,
   plot(pa,pm,'o',y,pm,':')
   ylabel('Sensor Output Voltage [V]')
   xlabel('Pressure [psi]')
   legend('Measured Output','Approx.')
   grid on
end

% Write the values of p to a file
dlmwrite(filename,p);
```

```
function press = sciib_post_proc(nb,bb,filename,ave_num);
%
% This function calculates the measured pressure
% given the individual channel data from an SCIIB
% system and the polynomial coefficients for the
% sensor used.
%
%
%      USAGE : press = sciib_post_proc(nb,bb,filename);
%
%              press : Vector containing the values of
%                      pressure measured by the system
%                 nb : Narrowband channel data
%                 bb : Broadband channel data
%           filename : Location of the polynomial
%                      coefficients
%            ave_num : Number of data samples to be
%                      averaged
%
%

% Load the filter and the polynomial
% coefficients
p   = dlmread(filename);

% Filter the channel data individually
n_b   = ave_filter(nb, ave_num);
b_b   = ave_filter(bb, ave_num);
press = ave_filter(nb./bb, ave_num);

% Perform calibration operation
press      = polyval(p,press);
```

```
% Script file used to call the functions for post-
% processing.

% Clear all buffers
clear all
close all
clc

% Define Variables
ave_num = 100;
sens_name = ['burst_2'];

% Load the sensor data and the LPF coeffs
psi    = dlmread('psi_2.log');
sensor = dlmread(['burst_2'.log']);

fiber_nb = sensor(1:2:end);
fiber_bb = sensor(2:2:end);

% Create time indices for plotting
t1 = 0:length(psi)-1;
t2 = (0:(length(fiber_nb)-1))/12500;

% Perform calibration operation
press = sciib_post_proc(fiber_nb,fiber_bb,'polyfit_p.log',ave_num);


% Plot results
figure,
plot(t2,press,t1,psi,'r'),
xlabel('Time [s]'),
ylabel('Pressure [psi]'),
grid on,
legend('SCIIB Sensor','Pressure calibration unit')
```